International Journal of Bifurcation and Chaos, Vol. 23, No. 8 (2013) 1350145 (33 pages)

DOI: 10.1142/S0218127413501459

SYNCHRONIZATION AND STABILIZATION OF MULTI-SCROLL INTEGER AND FRACTIONAL ORDER CHAOTIC ATTRACTORS GENERATED USING TRIGONOMETRIC FUNCTIONS

FEI XU
Department of Mathematics, Wilfrid Laurier University, Waterloo, Ontario N2L 3C5, Canada
fxu.feixu@gmail.com

PEI YU*
Department of Applied Mathematics, University of Western Ontario, London, Ontario N6A 5B7, Canada
pyu@uwo.ca

XIAOXIN LIAO
Department of Control Science and Engineering, Huazhong University of Science and Technology, Wuhan, Hubei 430074, P. R. China

Received February 6, 2013

Sigmoidal functions are usually used to characterize the behavior of dynamical systems, in particular, for neural networks. Recently, multilevel piecewise linear functions have been employed in cellular neural networks (CNN). In this paper, we first use the inverse trigonometric function, $\tan^{-1}(x)$, to generate a series of trigonometric functions to obtain one-, two- and three-directional multi-scroll integer and fractional order chaotic attractors. Then, based upon the properties of the chaotic systems, simple feedback control laws are designed to stabilize or synchronize the integer and fractional order chaotic systems. Numerical simulations are presented to demonstrate the applicability of theoretical predictions.

Keywords: Multi-scroll chaotic attractor; chaos synchronization; chaos control; Lyapunov function; inverse trigonometric function; fractional order chaotic attractor.

1. Introduction

Since the discovery of the Lorenz chaotic attractor [Lorenz, 1963], many researchers have been attracted to investigate fundamental dynamical properties of various chaotic systems (e.g. see [Rössler, 1976; Chua *et al.*, 1986; Chen & Ueta, 1999]). In order to generate different kinds of pseudo random series, one needs different multi-scroll chaotic attractors. Recently, many scientists have devoted themselves to the design and analysis of new multi-scroll chaotic attractors. The first double scroll chaotic attractor was found in Chua's Circuit [Chua *et al.*, 1986]. Since then, many researchers began to design new dynamical systems

*Author for correspondence

that can generate more chaotic scrolls. For instance, a generalized Chua's circuit which can generate n-scroll attractors was reported in 1999 [Yalcin *et al.*, 1999]. More recently, the research on one-directional(1-D)-n-scroll chaotic attractors has been extended to the study of two-directional(2-D)-$m \times n$-grid-scroll and three-directional(3-D)-$m \times n \times l$-grid-scroll chaotic attractors. A number of methods have been developed and reported in the literature (e.g. see [Lü *et al.*, 2004; Cafagna & Grassi, 2003; Yu *et al.*, 2005; Zhang & Yu, 2010]).

Besides the investigation of integer order chaotic systems, the existence of chaotic behavior in fractional order differential equation systems has also attracted researchers' attention [Li & Chen, 2004; Lu & Chen, 2006; Wu *et al.*, 2008; Huang *et al.*, 2012]. Recently, the control and synchronization of such fractional order chaotic systems have been studied [Wu *et al.*, 2008; Zhang *et al.*, 2012; Xu *et al.*, 2013].

In this paper, instead of the piecewise linear functions which are used in most circuits designs, we use the inverse trigonometric function, $\tan^{-1}(x)$, to generate a series of trigonometric functions to study chaotic behavior of dynamical systems. Since the function $\tan^{-1}(x)$ is similar to hyperbolic tangent function which is frequently used to characterize the behavior of neural networks, such a study may help understand complex dynamical behavior which exists in neural networks. In fact, multi-level piecewise linear functions have been recently employed in cellular neural networks (CNNs) [Forti, 2002]. It is thus necessary to explore the dynamical property of such systems. We will investigate how such a system with the $\tan^{-1}(x)$ function series generate 1-D-n-scroll, 2-D-$m \times n$-grid-scroll and 3-D-$m \times n \times l$-grid-scroll multi-scroll chaotic attractors. Then, based upon the properties of the chaotic systems, we design simple feedback control laws to globally exponentially stabilize or synchronize the chaotic systems. Further, we extend the study of integer order multi-scroll chaotic attractors to that of fractional order multi-scroll chaotic attractors. It is shown that the inverse trigonometric function, $\tan^{-1}(x)$, can be used to generate a series of fractional order, one-, two- or three-directional multi-scroll chaotic attractors. By designing simple feedback control laws, two such fractional order chaotic attractors can be synchronized. The fractional order chaotic systems can also be stabilized using simple feedback control laws. Numerical simulations are presented to demonstrate the applicability of theoretical predictions.

2. Definition of the $\tan^{-1}(x)$ Function Series

Multi-piecewise linear functions [see Fig. 1(a)] have been recently used in the study of cellular neural networks (CNNs) [Forti, 2002], which can be replaced by the following infinitely differentiable, $\tan^{-1}(x)$ function series:

$$f(x) = \frac{2}{\pi} \sum_{j=-r}^{s} \tan^{-1}(x + j\tau), \tag{1}$$

where the constant $\frac{2}{\pi}$ is used to normalize the function; the parameter τ is a positive real number, while the parameters r and s are non-negative

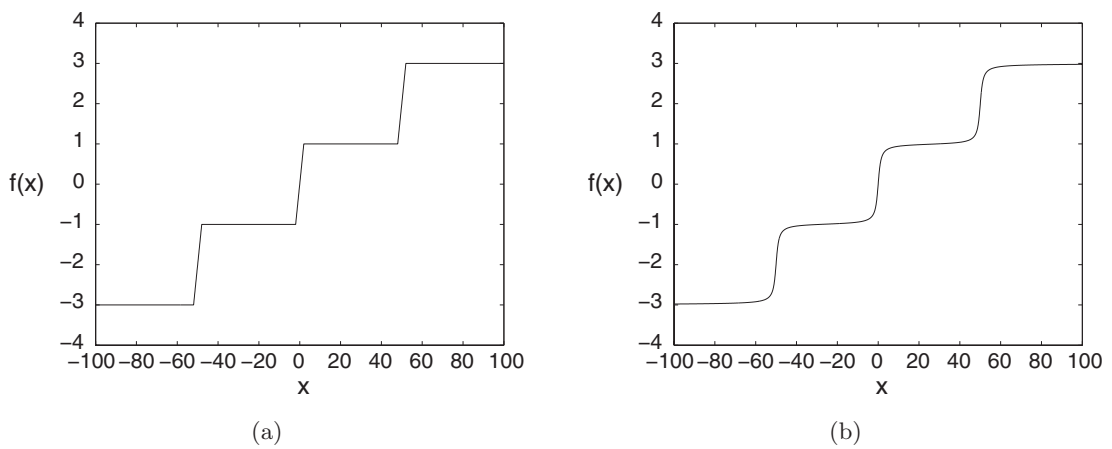

(a) (b)

Fig. 1. (a) A multi-piecewise linear function and (b) $f(x) = \frac{2}{\pi} \sum_{j=-1}^{1} \tan^{-1}(x + 50j)$.

integers. The function $f(x)$ is depicted in Fig. 1(b), which indeed smoothens the multilevel piecewise linear function [see Fig. 1(a)].

It will be shown in the next two sections that when the function $f(x)$ is added to a linear system, multi-scroll chaotic attractors can be generated and the maximal number of chaotic scrolls which can be obtained is $l = r + s + 2$. For example, when $r = s = 2$, the system can generate at most six chaotic scrolls.

3. Design of 1-D-n-Scroll Chaotic Attractors

The multi-scroll chaotic systems we will discuss can be obtained by adding the $\tan^{-1}(x)$ function series to the following linear system [Lü *et al.*, 2004]:

$$\begin{aligned} \dot{x} &= y, \\ \dot{y} &= z, \\ \dot{z} &= -ax - by - cz. \end{aligned} \tag{2}$$

Then the proposed model for 1-D chaos generator is given by

$$\begin{aligned} \dot{x} &= y, \\ \dot{y} &= z, \\ \dot{z} &= -ax - by - cz \\ &\quad + ad\left[(r-s) + \frac{2}{\pi}\sum_{j=-r}^{s}\tan^{-1}(x + j\tau)\right], \end{aligned} \tag{3}$$

where a, b, c and d take positive real values, s and r are non-negative integers, determining the maximum number of chaotic scrolls. For example, when $a = b = c = 0.65$, $d = 78.5398$, and $s = r = 0$, we obtain a double-scroll chaotic attractor, as shown in Fig. 2.

It is easy to see that for the above given parameter values, system (3) has three equilibrium points: $S_0 = (0, 0, 0)$ — a saddle point of index one, and $S_{1,2} = (\pm 78.5398, 0, 0)$ — two saddle points of index two. Therefore, $S_{1,2}$ are responsible for the generation of the double scrolls, whereas S_0 is responsible for the connection of the two chaotic scrolls. We can also compute the Lyapunov exponents of the system to verify the chaos. The Lyapunov exponents for this case are: $0.0987, -0.0009$ and -0.7478, indicating that the motion is chaotic.

In order for system (3) to generate 1-D-n-scroll chaotic attractors as many as possible, we first need to obtain equilibrium points of the system as many as possible. However, it is difficult to find the exact value of d such that the number of equilibrium points reaches its maximum. We know that $\lim_{x\to+\infty}\tan^{-1}(x) = \frac{\pi}{2}$ and $\lim_{x\to-\infty}\tan^{-1}(x) = -\frac{\pi}{2}$. To find the approximate value of d, we linearize the $\tan^{-1}(x)$ function, yielding

$$f(x) = \begin{cases} \dfrac{\pi}{2} & \text{when } x \geq \alpha, \\ \dfrac{\pi}{2\alpha}x, & \text{when } -\alpha < x < \alpha, \\ -\dfrac{\pi}{2}, & \text{when } x \leq -\alpha, \end{cases}$$

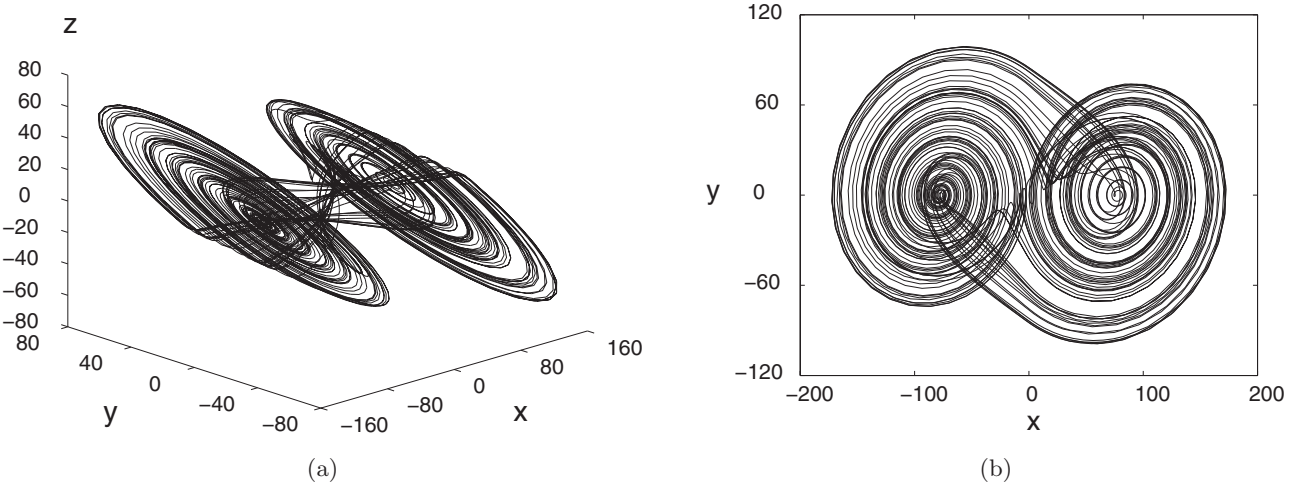

(a) (b)

Fig. 2. Simulated phase portrait of a double-scroll chaotic attractor for system (3) when $a = b = c = 0.65$, $d = 78.5398$, $r = s = 0$: (a) in the x–y–z space and (b) projected on the x–y plane.

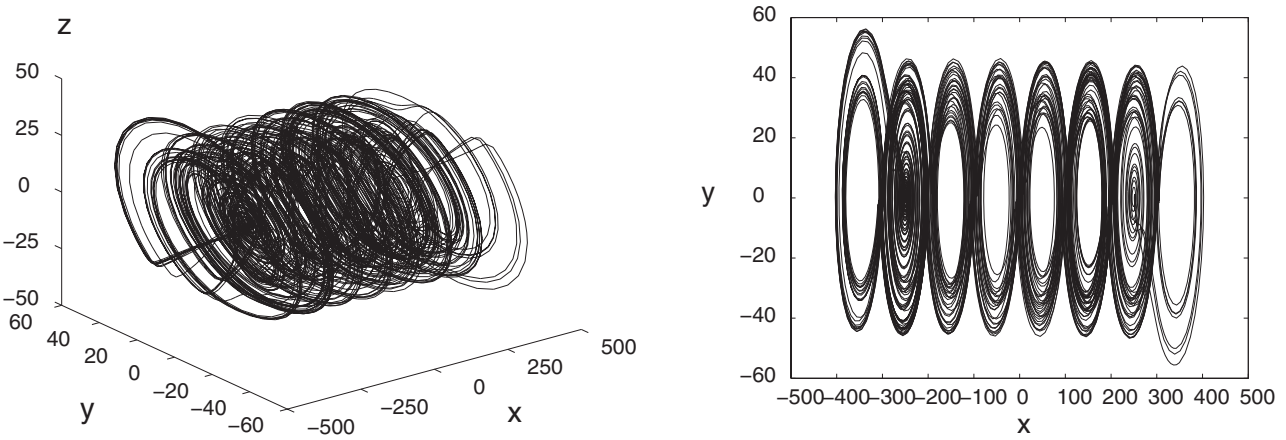

Fig. 3. Simulated phase portrait of 1-D-8-scroll chaotic attractor for system (4) when $a = b = c = 0.7$, $d = 50$, $r = s = 3$: (a) in the x–y–z space and (b) projected on the x–y plane.

where $\alpha > 0$. Using the above function to approximate $\tan^{-1}(x)$, it is easy to show that when $d = \frac{\tau}{2}$, the number of equilibrium points in the system is approximately maximized. Thus, system (3) becomes

$$\begin{aligned}\dot{x} &= y,\\ \dot{y} &= z,\\ \dot{z} &= -ax - by - cz\\ &\quad + a\frac{\tau}{2}\left[(r-s) + \sum_{j=-r}^{s}\frac{2}{\pi}\tan^{-1}(x + j\tau)\right],\end{aligned} \tag{4}$$

where a, b, c, and τ are positive real numbers. Obviously, when proper values of these coefficients are chosen, system (4) can have $(r+s+1)$ saddle points of index one (denoted by Γ_x) and $(r+s+2)$ saddle points of index two (denoted by Γ_x^*):

$$\begin{aligned}\Gamma_x &\approx \{s\tau, (s-1)\tau, \ldots, r\tau\},\\ \Gamma_x^* &\approx \left\{(2s+1)\frac{\tau}{2}, (2s-1)\frac{\tau}{2}, \ldots, (2r+1)\frac{\tau}{2}\right\},\end{aligned} \tag{5}$$

where the subscript x denotes the nonzero coordinate of the saddle points. Equilibrium points in the set Γ_x^*, which have corresponding eigenvalues $\lambda_1 < 0$ and $\lambda_{2,3} = \xi \pm \eta i$ with $\xi > 0$ and $\eta \neq 0$, are responsible for the generation of the $r + s + 2$ scrolls. Equilibrium points in the set Γ_x, which have corresponding eigenvalues $\lambda_1 > 0$ and $\lambda_{2,3} = \xi \pm \eta i$ with $\xi < 0$ and $\eta \neq 0$, are responsible for the connection of the $r + s + 2$ scrolls. Thus, system (4) can generate as many as $r + s + 2$ chaotic scrolls. For example, when $a = b = c = 0.7$, $d = 50$, $s = r = 3$, the corresponding $\tan^{-1}(x)$ function series can produce an 8-scroll chaotic attractor (see Fig. 3). The corresponding Lyapunov exponents for the system with these chosen parameter values are $0.0786, -0.0020, -0.7766$, implying that the motion is chaotic.

4. Design of 2-D-$m \times n$-Grid-Scroll Chaotic Attractors

To obtain 2-D-$m \times n$-grid-scroll chaotic attractors, we add two $\tan^{-1}(x)$ function series to the first and third equations of the same linear system (2) to obtain a new system:

$$\begin{aligned}\dot{x} &= y - \frac{\tau_2}{2}\left[(r_2 - s_2) + \sum_{j=-r_2}^{s_2}\frac{2}{\pi}\tan^{-1}(y + j\tau_2)\right],\\ \dot{y} &= z,\\ \dot{z} &= -ax - by - cz\\ &\quad + a\frac{\tau_1}{2}\left[(r_1 - s_1) + \sum_{j=-r_1}^{s_1}\frac{2}{\pi}\tan^{-1}(x + j\tau_1)\right]\\ &\quad + b\frac{\tau_2}{2}\left[(r_2 - s_2) + \frac{2}{\pi}\sum_{j=-r_2}^{s_2}\tan^{-1}(y + j\tau_2)\right],\end{aligned} \tag{6}$$

where a, b, c, τ_1 and τ_2 take positive real values, while r_1, r_2, s_1, s_2 are non-negative integers. Similarly, based on the study of equilibrium points, we

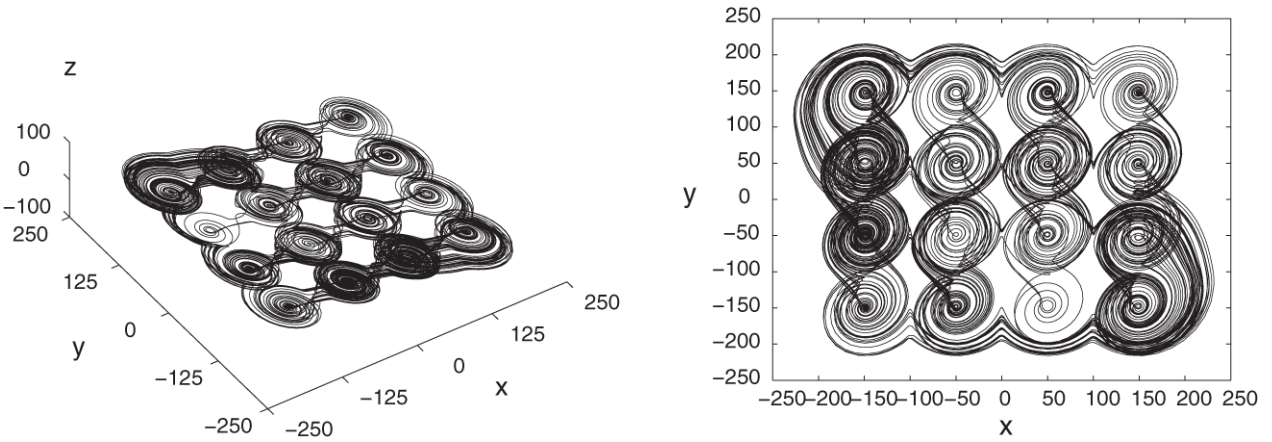

(a) (b)

Fig. 4. Simulated phase portrait of a 2-D-4 × 4-scroll chaotic attractor for system (6) when $a = b = c = 0.5$, $\tau_1 = \tau_2 = 100$, $r_1 = r_2 = s_1 = s_2 = 1$: (a) in the x–y–z space and (b) projected on the x–y plane.

can show that the system can generate an $m \times n$-grid-scroll chaotic attractor, where $m = r_1 + s_1 + 2$ and $n = r_2 + s_2 + 2$. For example, setting $a = b = c = 0.5$, $\tau_1 = \tau_2 = 100$, and $r_1 = r_2 = s_1 = s_2 = 1$ in system (6), we get a 4×4-grid-scroll chaotic attractors, as shown in Fig. 4. The corresponding Lyapunov exponents of the system are: $0.1194, -0.0018, -0.6177$, again indicating that the motion is chaotic.

5. Design of 3-D-$m \times n \times l$-Grid-Scroll Chaotic Attractors

3-D-$m \times n \times l$-grid-scroll chaotic attractors can be similarly generated by adding three $\tan^{-1}(x)$ function series to the linear system (2) to obtain the following system:

$$\dot{x} = y - \frac{\tau_2}{2}\left[(r_2 - s_2) + \sum_{j=-r_2}^{s_2} \frac{2}{\pi}\tan^{-1}(y + j\tau_2)\right],$$

$$\dot{y} = z - \frac{\tau_3}{2}\left[(r_3 - s_3) + \sum_{j=-r_3}^{s_3} \frac{2}{\pi}\tan^{-1}(z + j\tau_3)\right],$$

$$\dot{z} = -ax - by - cz + a\frac{\tau_1}{2}\left[(r_1 - s_1) + \sum_{j=-r_1}^{s_1} \frac{2}{\pi}\tan^{-1}(x + j\tau_1)\right]$$

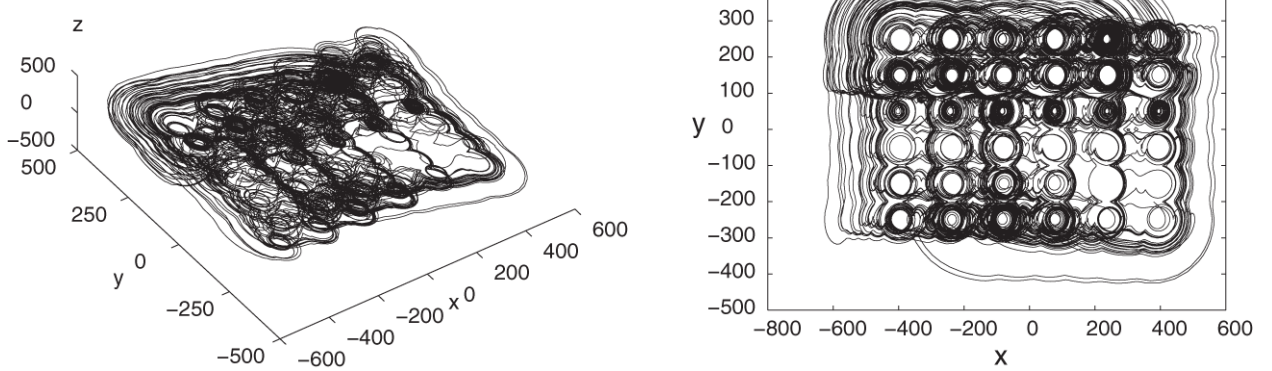

(a) (b)

Fig. 5. Simulated phase portrait of a 3-D-6 × 6 × 6-scroll chaotic attractor for system (7) when $a = b = c = 0.8$, $\tau_1 = 160$, $\tau_2 = 100$, $\tau_3 = 80$, and $r_1 = r_2 = r_3 = s_1 = s_2 = s_3 = 2$: (a) in the x–y–z space; (b) projected on the x–y plane; (c) projected on the x–z plane and (d) projected on the y–z plane.

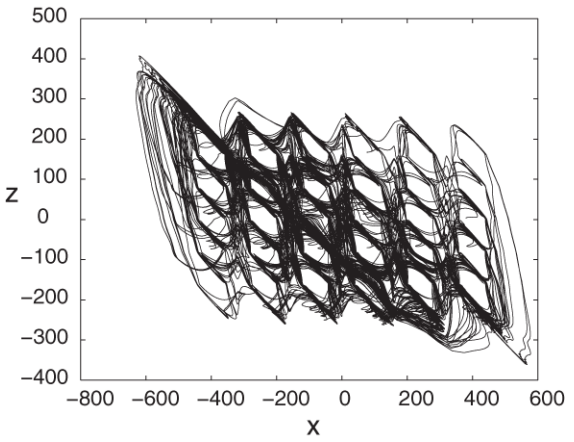

(c)

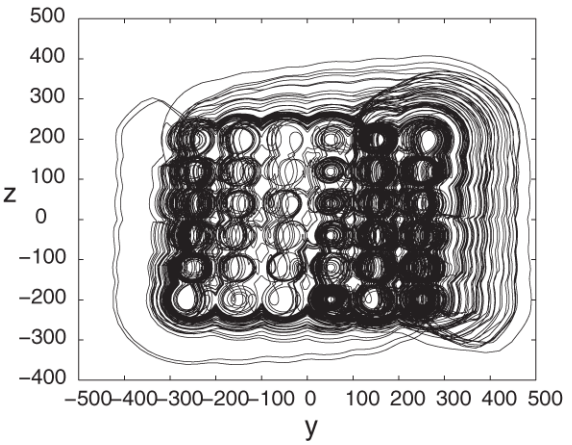

(d)

Fig. 5. (*Continued*)

$$+ b\frac{\tau_2}{2}\left[(r_2 - s_2) + \sum_{j=-r_2}^{s_2} \frac{2}{\pi}\tan^{-1}(y + j\tau_2)\right]$$
$$+ c\frac{\tau_3}{2}\left[(r_3 - s_3) + \sum_{j=-r_3}^{s_3} \frac{2}{\pi}\tan^{-1}(z + j\tau_3)\right], \tag{7}$$

where a, b, c, τ_1, τ_2 and τ_3 are positive real numbers, and r_1, r_2, r_3, s_1, s_2, s_3 are non-negative integers. This system can generate 3-D-$(r_1 + s_1 + 2) \times (r_2 + s_2 + 2) \times (r_3 + s_3 + 2)$ chaotic attractors, where $m = r_1 + s_1 + 2$, $n = r_2 + s_2 + 2$ and $l = r_3 + s_3 + 2$. For example, choosing $a = b = c = 0.8$, $\tau_1 = 160$, $\tau_2 = 100$, $\tau_3 = 80$, and $r_1 = r_2 = r_3 = s_1 = s_2 = s_3 = 2$ in system (7), we obtain a 3-D-$6 \times 6 \times 6$-grid-scroll chaotic attractor, as depicted in Fig. 5. The three Lyapunov exponents for this case are $0.1409, -0.0055, -0.6167$ showing that the motion is chaotic.

In the following sections, we consider the globally exponential synchronization for two same type of systems, which have been discussed in Secs. 3–5. We shall treat the stabilization of equilibrium points in chaos control as a special case of synchronization.

6. Synchronization and Stabilization of 1-D-*n*-Scroll Chaotic Attractors

Take system (3) as the driving system:

$$\dot{x}_d = y_d, \quad \dot{y}_d = z_d,$$
$$\dot{z}_d = -ax_d - by_d - cz_d + ad\left[(r - s) + \sum_{j=-r}^{s} \frac{2}{\pi}\tan^{-1}(x_d + j\tau)\right]. \tag{8}$$

Then, the corresponding driven system is

$$\begin{aligned}
\dot{x}_r &= y_r + u_1(x_d - x_r, y_d - y_r, z_d - z_r),\\
\dot{y}_r &= z_r + u_2(x_d - x_r, y_d - y_r, z_d - z_r),\\
\dot{z}_r &= -ax_r - by_r - cz_r\\
&\quad + ad\left[(r - s) + \sum_{j=-r}^{s} \frac{2}{\pi}\tan^{-1}(x_r + j\tau)\right]\\
&\quad + u_3(x_d - x_r, y_d - y_r, z_d - z_r),
\end{aligned} \tag{9}$$

where u_i's are continuous, linear or nonlinear functions of its variables, satisfying $u_i(0, 0, 0) = 0$, $i = 1, 2, 3$.

Let

$$e_x = x_d - x_r, \quad e_y = y_d - y_r, \quad e_z = z_d - z_r.$$

Then, the error system can be written as

$$\begin{aligned}
\dot{e}_x &= e_y - u_1(e_x, e_y, e_z),\\
\dot{e}_y &= e_z - u_2(e_x, e_y, e_z),\\
\dot{e}_z &= -ae_x - be_y - ce_z\\
&\quad + \sum_{j=-r}^{s} \frac{2ad}{\pi} f_j'(\xi_j)e_x - u_3(e_x, e_y, e_z),
\end{aligned} \tag{10}$$

where, by the intermediate value of theorem, $f_j'(\xi_j)e_x = \tan^{-1}(x_d + j\tau) - \tan^{-1}(x_r + j\tau)$ with

$\min(x_r, x_d) < \xi_j < \max(x_r, x_d)$. We will use the property $(\tan^{-1}(x))' = \frac{1}{1+x^2} \leq 1 < +\infty$ to study the globally exponential synchronization and globally exponential stability.

Assume that $X^* = (x^*, y^*, z^*)$ is any given equilibrium point of (3). Let $\overline{X} = X - X^* = (x - x^*, y - y^*, z - z^*)$. Then system (10) can be rewritten as

$$\begin{aligned} &\dot{\overline{x}} = \overline{y} - u_1(\overline{x}, \overline{y}, \overline{z}), \quad \dot{\overline{y}} = \overline{z} - u_2(\overline{x}, \overline{y}, \overline{z}), \\ &\dot{\overline{z}} = -a\overline{x} - b\overline{y} - c\overline{z} \\ &\qquad + \sum_{j=-r}^{s} \frac{2ad}{\pi} f_j'(\eta_j)\overline{x} - u_3(\overline{x}, \overline{y}, \overline{z}), \end{aligned} \tag{11}$$

where η_j is a number between x and x^*, and $f_j'(\eta_j)\overline{x} = \tan^{-1}(x + j\tau) - \tan^{-1}(x^* + j\tau)$.

Here, the basic idea we are applying is to choose the possibly simplest feedback controls u_1, u_2 and u_3 such that the zero solution of system (10) or system (11) is globally exponentially stabilized, and thus systems (8) and (9) are globally exponentially synchronized. Therefore, the equilibrium point $X = X^*$ is globally exponentially stabilized.

Definition 6.1. With properly chosen feedback controls u_i, $\forall\, x_d(0)$, $y_d(0)$, $z_d(0) \in R^3$ and corresponding $x_r(0)$, $y_r(0)$, $z_r(0) \in R^3$, if the zero solution of (10) is globally exponentially stabilized (globally asymptotically stabilized), then systems (8) and (9) are said to be globally exponentially synchronized (globally asymptotically synchronized).

Definition 6.2. With properly chosen feedback controls u_i, $\forall\, x_d(0)$, $y_d(0)$, $z_d(0) \in R^3$ and corresponding $x_r(0)$, $y_r(0)$, $z_r(0) \in R^3$, if the zero solution of (11) is globally exponentially stabilized (globally asymptotically stabilized), then the equilibrium point $X = X^*$ of system (3) is said to be globally exponentially stabilized (globally asymptotically stabilized).

Theorem 1. *For system (9), choose the following simple feedback control law*:

$$u_1 = \delta_x e_x, \quad u_2 = \delta_y e_y, \quad u_3 = \delta_z e_z. \tag{12}$$

Then, when one of the following conditions holds:

(1) $\delta_x > 1, \quad \delta_y > 1,$

$$\delta_z > a + b - c + \frac{2ad}{\pi}(s + r + 1);$$

(2) $\delta_x > a + \dfrac{2ad}{\pi}(s + r + 1), \quad \delta_y > b + 1,$

$$\delta_z > 1 - c;$$

the zero solution of (10) is globally exponentially stabilized, and thus systems (8) and (9) are globally exponentially synchronized.

Proof. We construct the following positive definite, radially unbounded vector Lyapunov function for system (10):

$$V = (|e_x|, |e_y|, |e_z|)^T.$$

Evaluating the Dini derivative of V along the solution orbits of system (10), we obtain

$$\begin{aligned} &\begin{pmatrix} D^+|e_x| \\ D^+|e_y| \\ D^+|e_z| \end{pmatrix}_{(10)} \\ &\leq \begin{bmatrix} -\delta_x & 1 & 0 \\ 0 & -\delta_y & 1 \\ a + \dfrac{2ad}{\pi}(s + r + 1) & b & -c - \delta_z \end{bmatrix} \\ &\quad \times \begin{pmatrix} |e_x| \\ |e_y| \\ |e_z| \end{pmatrix}. \end{aligned} \tag{13}$$

Next, consider the following comparison equation to (13):

$$\begin{aligned} \begin{pmatrix} \dot{\eta}_x \\ \dot{\eta}_y \\ \dot{\eta}_z \end{pmatrix} &= \begin{bmatrix} -\delta_x & 1 & 0 \\ 0 & -\delta_y & 1 \\ a + \dfrac{2ad}{\pi}(s + r + 1) & b & -c - \delta_z \end{bmatrix} \\ &\quad \times \begin{pmatrix} \eta_x \\ \eta_y \\ \eta_z \end{pmatrix} := A_1 \begin{pmatrix} \eta_x \\ \eta_y \\ \eta_z \end{pmatrix}, \end{aligned} \tag{14}$$

which has the solution:

$$\begin{pmatrix} \eta_x(t) \\ \eta_y(t) \\ \eta_z(t) \end{pmatrix} = e^{A_1(t - t_0)} \begin{pmatrix} \eta_x(t_0) \\ \eta_y(t_0) \\ \eta_z(t_0) \end{pmatrix}.$$

From any of the conditions of Theorem 1 we know that A_1 is a Hurwitz matrix [Liao, 2001].

Hence, there exist constants $M_1 \geq 1$ and $\alpha_1 > 0$ such that

$$\|e^{A_1(t-t_0)}\| \leq M_1 e^{-\alpha_1(t-t_0)}.$$

By the comparison principal, we have

$$\left\| \begin{pmatrix} |e_x(t)| \\ |e_y(t)| \\ |e_z(t)| \end{pmatrix} \right\| \leq \left\| \begin{pmatrix} \eta_x(t) \\ \eta_y(t) \\ \eta_z(t) \end{pmatrix} \right\|$$

$$\leq M_1 e^{-\alpha_1(t-t_0)} \left\| \begin{pmatrix} \eta_x(t_0) \\ \eta_y(t_0) \\ \eta_z(t_0) \end{pmatrix} \right\|, \quad (15)$$

indicating that the zero solution of system (10) is globally exponentially stabilized. Therefore, by Definition 6.1 we know that systems (8) and (9) are globally exponentially synchronized. ■

Next, we present a numerical example to demonstrate the applicability of Theorem 1. Here we choose $\delta_x = \delta_y = 1.05$ and $\delta_z = 34$, satisfying the conditions in Theorem 1. It is shown (see Fig. 6) that, under the proposed control, the zero solution of system (10) is globally exponentially stabilized and thus systems (8) and (9) are globally exponentially synchronized.

Remark 6.1. It should be noted that the control law given in Eq. (12) is not the so-called "cancelation" controller, since it does not cancel any terms on the right-hand side of the error system (10), nor that of the controlled system (9). In fact, substituting the feedback control (12) into Eq. (9) yields the controlled system:

$$\begin{aligned} \dot{x}_r &= y_r + \delta_x(x_d - x_r), \\ \dot{y}_r &= z_r + \delta_y(y_d - y_r), \\ \dot{z}_r &= -ax_r - by_r - cz_r + \delta_z(z_d - z_r) \\ &\quad + ad\left[(r-s) + \sum_{j=-r}^{s} \frac{2}{\pi} \tan^{-1}(x_r + j\tau)\right]. \end{aligned} \quad (16)$$

It is easy to see that the original terms y_r and z_r in the first two equations of (16) are not canceled by the control terms. For the third equation, since the control gain δ_z is either greater than $a + b - c + \frac{2ad}{\pi}(s + r + 1)$ or greater than $1 - c$, the control term $-\delta_z z_r$ does not cancel the original term $-cz_r$.

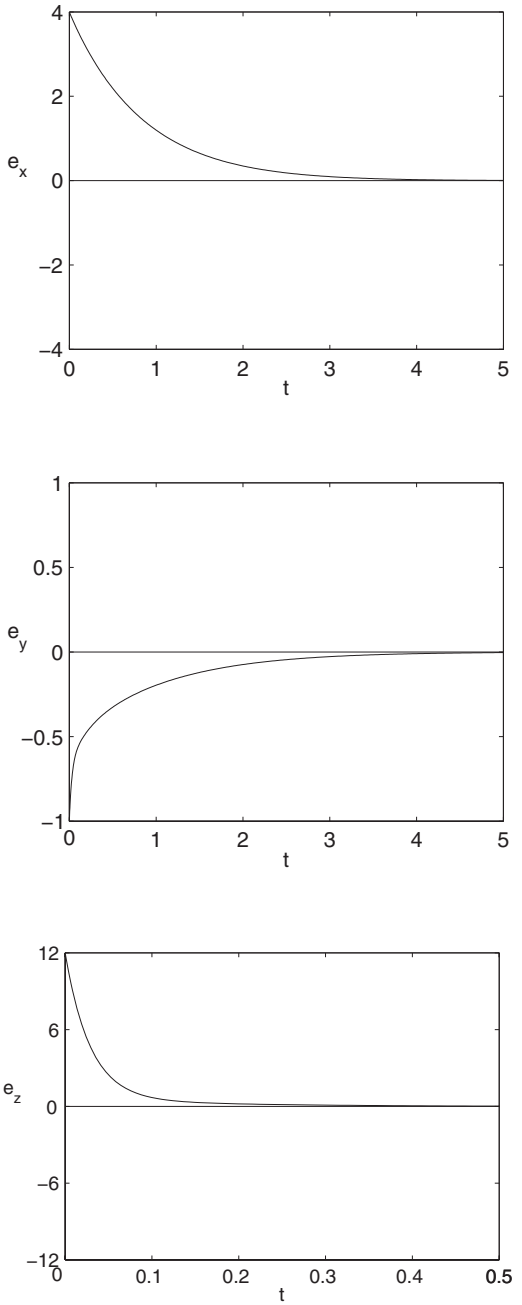

Fig. 6. Time history of the error system (10) for $a = b = c = 0.65$, $d = 78.5398$, $r = s = 0$ with the control law given in Theorem 1, using the initial conditions, $x_d(0) = 5$, $y_d(0) = 1$, $z_d(0) = 15$ and $x_r(0) = 1$, $y_r(0) = 2$, $z_r(0) = 3$, when $\delta_x = \delta_y = 1.05$ and $\delta_z = 34$.

However, if we choose the following linear control law:

$$\begin{aligned} u_1 &= e_y + e_x, \\ u_2 &= e_z + e_y, \\ u_3 &= -(ae_x + be_y + ce_z) + e_z, \end{aligned} \quad (17)$$

then the linear terms on the right-hand side of the error system (10) are all canceled and we obtain

$$\begin{aligned} \dot{e}_x &= -e_x, \\ \dot{e}_y &= -e_y, \\ \dot{e}_x &= -e_z + \sum_{j=-r}^{s} \frac{2ad}{\pi} f_j'(\xi_j) e_x. \end{aligned} \tag{18}$$

It is easy to see that system (18) is globally asymptotically stable. Substituting this control into the corresponding system (9) would cancel all the linear terms on the right-hand side of this system. Hence, control design (17) is indeed a cancelation control law, which is not desirable from the view point of control theory and should not be adopted.

Corollary 6.1. *For any given equilibrium point $X = X^*$ of system (8), choose the following feedback control law*:

$$u_1 = \delta_x \overline{x}, \quad u_2 = \delta_y \overline{y}, \quad u_3 = \delta_z \overline{z}. \tag{19}$$

Then if one of the following conditions is satisfied:

(1) $\delta_x > 1, \quad \delta_y > 1,$

$$\delta_z > a + b - c + \frac{2ad}{\pi}(s + r + 1);$$

(2) $\delta_x > a + \dfrac{2ad}{\pi}(s + r + 1), \quad \delta_y > b + 1,$

$$\delta_z > 1 - c;$$

$X^* = (x^*, y^*, z^*)$ can be globally exponentially stabilized.

To demonstrate the use of Corollary 6.1, we present a numerical example by choosing $\delta_x = \delta_y = 1.05$ and $\delta_z = 34$, which satisfy the conditions in Corollary 6.1. It is shown [see Fig. 7(a)] that under the proposed control law, all solution orbits of system (11) globally exponentially converge to the equilibrium point $(0, 0, 0)$.

Remark 6.2. System (8) may have multiple equilibrium points. However, when the feedback control law: $u_1 = \delta_x \overline{x}$, $u_2 = \delta_y \overline{y}$ and $u_3 = \delta_z \overline{z}$ is applied, which is designed for the equilibrium point $X^* = (x^*, y^*, z^*)$, all the other equilibrium points disappear. The only equilibrium point used for the control design is globally exponentially stabilized.

Theorem 2. *Choose the feedback control law*:

$$u_1 = \delta_x e_x, \quad u_2 = \delta_y e_y, \quad u_3 = \delta_z e_z,$$

for system (9). Then under the following conditions:

$$\delta_x > \frac{1}{2} + \frac{a}{2b} + \frac{ad}{\pi b}(s + r + 1),$$

$$\delta_y > \frac{1}{2},$$

$$\delta_z > -c + \frac{ad}{\pi}(s + r + 1) + \frac{a}{2},$$

the zero solution of the error system (10) is globally exponentially stabilized, and thus the two

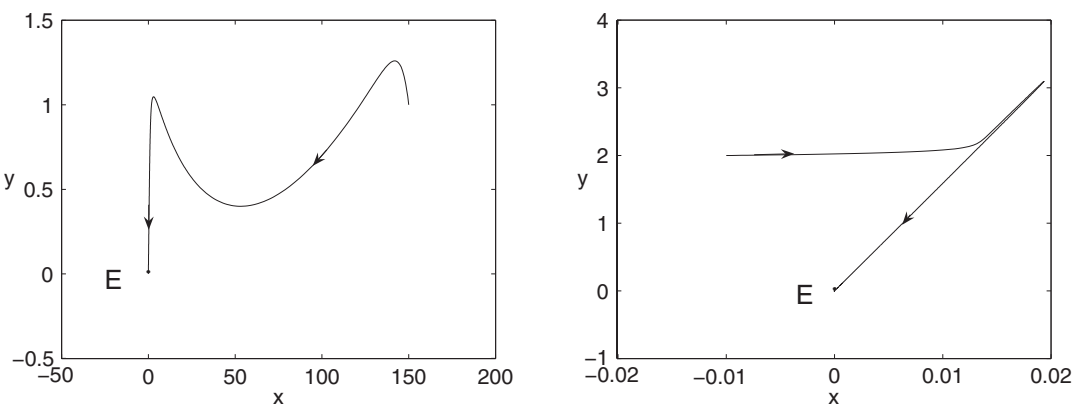

(a) (b)

Fig. 7. (a) Trajectory of a double-scroll chaotic attractor for system (11) when $a = b = c = 0.65$, $d = 78.5398$, $r = s = 0$ with the control law given in Corollary 6.1-1 for $\delta_x = \delta_y = 1.05$ and $\delta_z = 34$ convergent to the equilibrium point, $E : (0, 0, 0)$ and (b) trajectory of 1-D-8-scroll chaotic attractor for system (11) when $a = b = c = 0.7$, $d = 50$, $r = s = 3$ with the control law given in Corollary 6.3 for $\delta_x = 160$, $\delta_y = 1.8$ and $\delta_z = 0.5$ convergent to the equilibrium point, $E : (0, 0, 0)$.

systems (8) and (9) are globally exponentially synchronized.

Proof. Construct the positive definite, radially unbounded Lyapunov function for system (10):

$$V = \frac{1}{2}\left(e_x^2 + e_y^2 + \frac{e_z^2}{b}\right) = \begin{pmatrix} e_x \\ e_y \\ e_z \end{pmatrix}^T P \begin{pmatrix} e_x \\ e_y \\ e_z \end{pmatrix}.$$

Let $\lambda_m(P)$ and $\lambda_M(P)$ denote the minimum and maximum eigenvalues of

$$P = \begin{bmatrix} \frac{1}{2} & 0 & 0 \\ 0 & \frac{1}{2} & 0 \\ 0 & 0 & \frac{1}{2b} \end{bmatrix},$$

respectively. Then, we have

$$\begin{aligned} \left.\frac{dV}{dt}\right|_{(10)} &\le e_x e_y - \delta_x e_x^2 - \delta_y e_y^2 - \frac{a}{b} e_x e_z - \frac{c}{b} e_z^2 + \frac{2ad}{\pi b}|e_x e_z|(r+s+1) - \frac{1}{b}\delta_z e_z^2 \\ &\le |e_x e_y| - \delta_x e_x^2 - \delta_y e_y^2 + \frac{a}{b}|e_x e_z| - \frac{c}{b} e_z^2 + \frac{2ad}{\pi b}|e_x e_z|(r+s+1) - \frac{1}{b}\delta_z e_z^2 \\ &\le \begin{pmatrix} |e_x| \\ |e_y| \\ |e_z| \end{pmatrix}^T \begin{bmatrix} -\delta_x & \frac{1}{2} & \frac{a}{2b} + \frac{ad}{b\pi}(r+s+1) \\ \frac{1}{2} & -\delta_y & 0 \\ \frac{a}{2b} + \frac{ad}{b\pi}(r+s+1) & 0 & -\frac{c+\delta_z}{b} \end{bmatrix} \begin{pmatrix} |e_x| \\ |e_y| \\ |e_z| \end{pmatrix} \\ &:= \begin{pmatrix} |e_x| \\ |e_y| \\ |e_z| \end{pmatrix}^T A_2 \begin{pmatrix} |e_x| \\ |e_y| \\ |e_z| \end{pmatrix} \\ &\le \lambda_M(A_2)(e_x^2 + e_y^2 + e_z^2), \end{aligned} \tag{20}$$

where $\lambda_M(A_2)$ is the maximum eigenvalue of A_2. It follows from the conditions of Theorem 2 that $\lambda_M(A_2) < 0$. Thus,

$$\frac{dV}{dt} \le \lambda_M(A_2)\frac{\lambda_M(P)}{\lambda_M(P)}(e_x^2 + e_y^2 + e_z^2) \le \frac{\lambda_M(A_2)}{\lambda_M(P)} V,$$

implying that

$$V(X(t)) \le V(X(t_0)) e^{\frac{\lambda_M(A_2)}{\lambda_M(P)}(t-t_0)}.$$

Therefore,

$$\begin{aligned} &e_x^2(t) + e_y^2(t) + e_z^2(t) \\ &\quad \le \frac{V(X(t))}{\lambda_m(P)} \le \frac{V(X(t_0))}{\lambda_m(P)} e^{\frac{\lambda_M(A_2)}{\lambda_M(P)}(t-t_0)}, \end{aligned} \tag{21}$$

indicating that the zero solution of (10) is globally exponentially stabilized, and thus systems (8) and (9) are globally exponentially synchronized. ■

Corollary 6.2. *For any given equilibrium point $X = X^*$ of system (8), choose the feedback control law*:

$$u_1 = \delta_x \overline{x}, \quad u_2 = \delta_y \overline{y}, \quad u_3 = \delta_z \overline{z}.$$

If

$$\delta_x > \frac{1}{2} + \frac{a}{2b} + \frac{ad}{\pi b}(s+r+1), \quad \delta_y > \frac{1}{2},$$

$$\delta_z > -c + \frac{ad}{\pi}(s+r+1) + \frac{a}{2},$$

then the equilibrium point of (8), $X = X^*$, is globally exponentially stabilized.

The proof of Corollary 6.2 is similar to that for Theorem 2, and thus omitted.

Theorem 3. *Take the same feedback control law*:

$$u_1 = \delta_x e_x, \quad u_2 = \delta_y e_y, \quad u_3 = \delta_z e_z,$$

for system (9). Then, when

$$\delta_x > a + \frac{2ad}{\pi}(r + s + 1),$$
$$\delta_y = 1 + b, \quad \delta_z = 1 - c,$$

the zero solution of (10) is globally exponentially stabilized, i.e. the two systems (8) and (9) are globally exponentially synchronized.

Proof. Construct the positive definite, radially unbounded Lyapunov function for Eq. (10):

$$V = |e_x| + |e_y| + |e_z|.$$

Then we obtain

$$\begin{aligned} D^+V|_{(10)} &= \dot{e}_x \operatorname{sign} e_x + \dot{e}_y \operatorname{sign} e_y + \dot{e}_z \operatorname{sign} e_z \\ &\le |e_y| + |e_z| - \delta_x|e_x| - \delta_y|e_y| - \delta_z|e_z| \\ &\quad - c|e_z| + \frac{2ad(r+s+1)}{\pi}|e_x| \\ &\quad + a|e_x| + b|e_y| \\ &= \left(-\delta_x + a + \frac{2ad(r+s+1)}{\pi}\right)|e_x| \\ &\quad + (-\delta_y + b + 1)|e_y| \\ &\quad + (-\delta_z - c + 1)|e_z| \\ &= \left(-\delta_x + a + \frac{2ad(r+s+1)}{\pi}\right)|e_x|, \end{aligned} \tag{22}$$

implying that the zero solution of (10) is globally exponentially stabilized with respect to the partial variable e_x.

Now we consider the coefficient matrix of the linear part of system (10) with the feedback control law given in Theorem 3:

$$A_3 = \begin{bmatrix} -\delta_x & 1 & 0 \\ 0 & -\delta_y & 1 \\ -a & -b & -1 \end{bmatrix}$$

from which we obtain the characteristic polynomial:

$$\begin{aligned} &\det(\lambda I_3 - A_3) \\ &= \det\begin{bmatrix} \lambda + \delta_x & -1 & 0 \\ 0 & \lambda + 1 + b & -1 \\ a & b & \lambda + 1 \end{bmatrix} \\ &= \lambda^3 + (b + 2 + \delta_x)\lambda^2 \\ &\quad + [\delta_x(b+2) + 2b + 1]\lambda + \delta_x(2b+1) + a \\ &:= \lambda^3 + p\lambda^2 + q\lambda + r. \end{aligned}$$

It is well known that the sufficient and necessary conditions for A_3 being a Hurwitz matrix are

$$0 < p \quad \text{and} \quad 0 < r < pq.$$

Setting $a = b$, we obtain

$$\begin{aligned} pq &= (b + 2 + \delta_x)[\delta_x(b+2) + 2b + 1] \\ &= (b+2)(b+1) + \delta_x(b+2)^2 + b(b+2) \\ &\quad + \delta_x(b+1) + \delta_x^2(b+2) + b\delta_x \\ &> \delta_x(2b+1) + b = r > 0. \end{aligned} \tag{23}$$

Equation (23) shows that A_3 is a Hurwitz matrix.

On the other hand, the solution of (10) can be written as

$$\begin{aligned} \begin{pmatrix} e_x(t) \\ e_y(t) \\ e_z(t) \end{pmatrix} &= e^{A_3(t-t_0)} \begin{pmatrix} e_x(t_0) \\ e_y(t_0) \\ e_z(t_0) \end{pmatrix} \\ &\quad + \int_{t_0}^{t} e^{A_3(t-\tau)} \begin{pmatrix} 0 \\ 0 \\ \displaystyle\sum_{j=-r}^{s} \frac{2ad}{\pi} f'(\xi) e_x(\tau) \end{pmatrix} d\tau. \end{aligned}$$

Since A_3 is a Hurwitz matrix, there exist constants $M_1 \ge 1$ and $\alpha_1 > 0$ such that

$$\|e^{A_3(t-t_0)}\| \le M_1 e^{-\alpha_1(t-t_0)}.$$

Hence,

$$\left\|\begin{pmatrix} e_x(t) \\ e_y(t) \\ e_z(t) \end{pmatrix}\right\| \le M_1 \left\|\begin{pmatrix} e_x(t_0) \\ e_y(t_0) \\ e_z(t_0) \end{pmatrix}\right\| e^{-\alpha_1(t-t_0)} + \int_{t_0}^{t} M_1 e^{-\alpha_1(t-\tau)} \frac{2ad}{\pi}(s+r+1) \times \|e_x(\tau)\| d\tau.$$

Using the property that $e_x(t) \to 0$ as $t \to \infty$, we can prove that $\forall\, \varepsilon > 0$, $\exists\, \sigma_1 > 0$, when $\|(e_x(t_0), e_y(t_0), e_z(t_0))^T\| \le \sigma_1$,

$$M_1 \left\|\begin{pmatrix} e_x(t_0) \\ e_y(t_0) \\ e_z(t_0) \end{pmatrix}\right\| e^{-\alpha_1(t-t_0)} < \frac{\varepsilon}{3}.$$

In addition, for any $t_1 > t_0$, when $\|(e_x(t_0), e_y(t_0), e_z(t_0))^T\| \le \sigma_1$, we have

$$\int_{t_0}^{t_1} M_1 e^{-\alpha_1(t-\tau)} \frac{2ad}{\pi}(s+r+1)\|e_x(\tau)\| d\tau < \frac{\varepsilon}{3}$$

and

$$\int_{t_1}^{t} M_1 e^{-\alpha_1(t-\tau)} \frac{2ad}{\pi}(s+r+1)\|e_x(\tau)\| d\tau < \frac{\varepsilon}{3}.$$

Thus,

$$\begin{aligned} &\left\|\begin{pmatrix} e_x(t) \\ e_y(t) \\ e_z(t) \end{pmatrix}\right\| \\ &\le M_1 \left\|\begin{pmatrix} e_x(t_0) \\ e_y(t_0) \\ e_z(t_0) \end{pmatrix}\right\| e^{-\alpha_1(t-t_0)} \\ &\quad + \int_{t_0}^{t_1} M_1 e^{-\alpha_1(t-\tau)} \frac{2ad}{\pi}(s+r+1)\|e_x(\tau)\| d\tau \\ &\quad + \int_{t_1}^{t} M_1 e^{-\alpha_1(t-\tau)} \frac{2ad}{\pi}(s+r+1)\|e_x(\tau)\| d\tau \\ &< \frac{\varepsilon}{3} + \frac{\varepsilon}{3} + \frac{\varepsilon}{3} = \varepsilon. \end{aligned}$$

For any $(e_x(t_0), e_y(t_0), e_z(t_0))^T \in R^3$, it is easy to see that

$$\begin{aligned} &\lim_{t\to\infty} M_1 \left\|\begin{pmatrix} e_x(t_0) \\ e_y(t_0) \\ e_z(t_0) \end{pmatrix}\right\| e^{-\alpha_1(t-t_0)} \\ &\quad + \lim_{t\to\infty} \int_{t_0}^{t} M_1 e^{-\alpha_1(t-\tau)} \frac{2ad}{\pi}(s+r)\|e_x(\tau)\| d\tau \\ &= 0. \end{aligned} \tag{24}$$

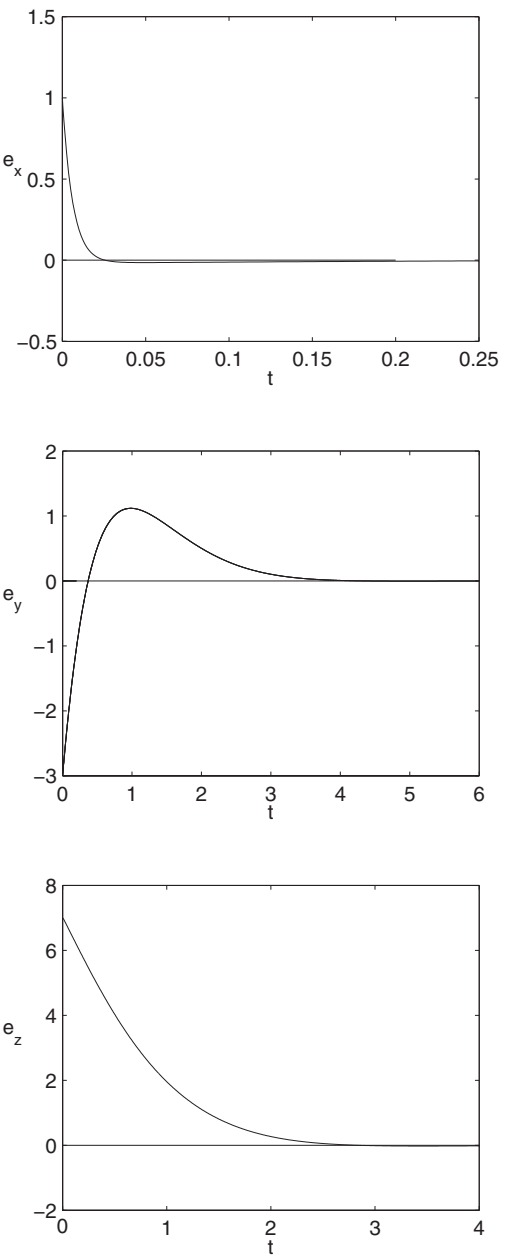

Fig. 8. Time history of the error system (10) for $a = b = c = 0.7$, $d = 50$, $r = s = 3$ with the control law given in Theorem 3, using the initial conditions, $x_d(0) = 2$, $y_d(0) = 2$, $z_d(0) = 10$ and $x_r(0) = 1$, $y_r(0) = 5$, $z_r(0) = 3$, when $\delta_x = 160$, $\delta_y = 1.8$ and $\delta_z = 0.5$.

Hence, the zero solution of (10) is globally asymptotically stabilized, and so systems (8) and (9) are globally exponentially synchronized. ■

To demonstrate the applicability of Theorem 3, we show a numerical example. Choose $\delta_x = 160$, $\delta_y = 1.8$ and $\delta_z = 0.5$, satisfying the conditions in this theorem. The simulations depicted in Fig. 8 clearly indicate that the zero solution of system (10) is globally exponentially stabilized and thus systems (8) and (9) are globally exponentially synchronized.

Corollary 6.3. *For any equilibrium point $X = X^*$ of system (8), choose feedback control law*:

$$u_1 = \delta_x \overline{x}, \quad u_2 = \delta_y \overline{y}, \quad u_3 = \delta_z \overline{z}.$$

Then, when

$$\delta_x > a + \frac{2ad}{\pi}(r + s + 1),$$

$$\delta_y = 1 + b, \quad \delta_z = 1 - c,$$

X^* can be globally exponentially stabilized.

A numerical simulation example is shown in Fig. 7(b) to illustrate the usefulness of Corollary 6.3. As $\delta_x = 160$, $\delta_y = 1.8$ and $\delta_z = 0.5$ satisfying the condition of Corollary 6.3, the solution orbit of system (11) globally exponentially converges to the equilibrium point $(0, 0, 0)$.

7. Synchronization and Stabilization of 2-D-$m \times n$-Grid-Scroll Chaotic Attractors

In this section, we consider 2-D chaotic attractors. Assume that the driving system is given by

$$\begin{aligned}
\dot{x}_d &= y_d - \frac{\tau_2}{2}\left[(r_2 - s_2) + \sum_{j=-r_2}^{s_2} \frac{2}{\pi}\tan^{-1}(y_d + j\tau_2)\right],\\
\dot{y}_d &= z_d,\\
\dot{z}_d &= -ax_d - by_d - cz_d\\
&\quad + \frac{a\tau_1}{2}\left[(r_1 - s_1) + \sum_{j=-r_1}^{s_1} \frac{2}{\pi}\tan^{-1}(x_d + j\tau_1)\right]\\
&\quad + \frac{b\tau_2}{2}\left[(r_2 - s_2) + \sum_{j=-r_2}^{s_2} \frac{2}{\pi}\tan^{-1}(y_d + j\tau_2)\right],
\end{aligned} \tag{25}$$

and the corresponding driven system is

$$\begin{aligned}
\dot{x}_r &= y_r - \frac{\tau_2}{2}\left[(r_2 - s_2) + \sum_{j=-r_2}^{s_2} \frac{2}{\pi}\tan^{-1}(y_r + j\tau_2)\right]\\
&\quad + u_1(e_x, e_y, e_z),\\
\dot{y}_r &= z_r + u_2(e_x, e_y, e_z),\\
\dot{z}_r &= -ax_r - by_r - cz_r\\
&\quad + \frac{a\tau_1}{2}\left[(r_1 - s_1) + \sum_{j=-r_1}^{s_1} \frac{2}{\pi}\tan^{-1}(x_r + j\tau_1)\right]\\
&\quad + \frac{b\tau_2}{2}\left[(r_2 - s_2) + \sum_{j=-r_2}^{s_2} \frac{2}{\pi}\tan^{-1}(y_r + j\tau_2)\right]\\
&\quad + u_3(e_x, e_y, e_z).
\end{aligned} \tag{26}$$

Then the error system can be written as

$$\begin{aligned}
\dot{e}_x &= e_y - \frac{\tau_2}{\pi}\sum_{j=-r_2}^{s_2} f'_{2j}(\xi_{2j})e_y - u_1(e_x, e_y, e_z),\\
\dot{e}_y &= e_z - u_2(e_x, e_y, e_z),\\
\dot{e}_z &= -ae_x - be_y - ce_z + \frac{a\tau_1}{\pi}\sum_{j=-r_1}^{s_1} f'_{1j}(\xi_{1j})e_x\\
&\quad + \frac{b\tau_2}{\pi}\sum_{j=-r_2}^{s_2} f'_{2j}(\xi_{2j})e_y - u_3(e_x, e_y, e_z),
\end{aligned} \tag{27}$$

where, $f'_{1j}(\xi_{1j})e_x = \tan^{-1}(x_d + j\tau_1) - \tan^{-1}(x_r + j\tau_1)$, $\min(x_r, x_d) < \xi_{1j} < \max(x_r, x_d)$, $f'_{2j}(\xi_{2j})e_y = \tan^{-1}(y_d + j\tau_2) - \tan^{-1}(y_r + j\tau_2)$, and $\min(y_r, y_d) < \xi_{2j} < \max(y_r, y_d)$.

Theorem 4. *In system (26), choose the following control law*:

$$u_1 = \delta_x e_x, \quad u_2 = \delta_y e_y, \quad u_3 = \delta_z e_z.$$

If one of the following conditions is satisfied:

(1) $\delta_x > 1 + \frac{\tau_2}{\pi}(s_2 + r_2 + 1), \quad \delta_y > 1,$

$$\delta_z > a + \frac{a\tau_1}{\pi}(s_1 + r_1 + 1) + b + \frac{b\tau_2}{\pi}(s_2 + r_2 + 1) - c;$$

(2) $\delta_x > a + \dfrac{a\tau_1}{\pi}(s_1 + r_1 + 1)$,

$\delta_y > 1 + \dfrac{\tau_2}{\pi}(s_2 + r_2 + 1) + b + \dfrac{b\tau_2}{\pi}(s_2 + r_2 + 1)$,

$\delta_z > 1 - c$;

then the zero solution of (27) is globally exponentially stabilized, and thus systems (25) and (26) are globally exponentially synchronized.

Proof. Construct the positive definite, radially unbounded vector Lyapunov function:

$$V = (|e_x|, |e_y|, |e_z|)^T,$$

and then we have

$$D^+V|_{(27)} = \begin{pmatrix} D^+|e_x| \\ D^+|e_y| \\ D^+|e_z| \end{pmatrix}_{(27)} \leq \begin{bmatrix} -\delta_x & 1 + \dfrac{\tau_2}{\pi}(s_2 + r_2 + 1) & 0 \\ 0 & -\delta_y & 1 \\ a + \dfrac{a\tau_1}{\pi}(s_1 + r_1 + 1) & b + \dfrac{b\tau_2}{\pi}(s_2 + r_2 + 1) & -\delta_z - c \end{bmatrix} \begin{pmatrix} |e_x| \\ |e_y| \\ |e_z| \end{pmatrix}$$

$$:= A_4 \begin{pmatrix} |e_x| \\ |e_y| \\ |e_z| \end{pmatrix}. \tag{28}$$

Consider the comparison equation of (28), given by

$$\begin{pmatrix} \dot{\eta}_x \\ \dot{\eta}_y \\ \dot{\eta}_z \end{pmatrix} = \begin{bmatrix} -\delta_x & 1 + \dfrac{\tau_2}{\pi}(s_2 + r_2 + 1) & 0 \\ 0 & -\delta_y & 1 \\ a + \dfrac{a\tau_1}{\pi}(s_1 + r_1 + 1) & b + \dfrac{b\tau_2}{\pi}(s_2 + r_2 + 1) & -\delta_z - c \end{bmatrix} \begin{pmatrix} \eta_x \\ \eta_y \\ \eta_z \end{pmatrix} := A_4 \begin{pmatrix} \eta_x \\ \eta_y \\ \eta_z \end{pmatrix}. \tag{29}$$

The solution of Eq. (29) is

$$\begin{pmatrix} \eta_x(t) \\ \eta_y(t) \\ \eta_z(t) \end{pmatrix} = e^{A_4(t-t_0)} \begin{pmatrix} \eta_x(t_0) \\ \eta_y(t_0) \\ \eta_z(t_0) \end{pmatrix}.$$

From the given conditions we know that A_4 is a Hurwitz matrix. Thus, there exist constants $M_4 \geq 1$ and $\alpha_4 > 0$ satisfying

$$\|e^{A_4(t-t_0)}\| \leq M_4 e^{-\alpha_4(t-t_0)}.$$

By the comparison principle we have that

$$\begin{aligned} &\|(|e_x(t)|, |e_y(t)|, |e_z(t)|)^T\| \\ &\quad \leq \|(\eta_x(t), \eta_y(t), \eta_z(t))^T\| \\ &\quad \leq M_4 e^{-\alpha_4(t-t_0)} \|(\eta_x(t_0), \eta_y(t_0), \eta_z(t_0))^T\|, \end{aligned} \tag{30}$$

implying that the conclusion of Theorem 4 is true. ■

To demonstrate the applicability of Theorem 4, we present two numerical examples here. For the first condition of Theorem 4, take $\delta_x = 100$, $\delta_y = 1.05$ and $\delta_z = 100$. It is shown (see Fig. 9) that under the proposed control law, the zero solution of (27) is globally exponentially stabilized, thus systems (25) and (26) are globally exponentially synchronized. For the second condition, we choose $\delta_x = 50$, $\delta_y = 150$ and $\delta_z = 0.8$. Similar result is obtained, as shown in Fig. 10.

Corollary 7.1. *For any given equilibrium point $X = X^*$ of system (25), if we choose the following feedback control law*:

$$u_1 = \delta_x \overline{x}, \quad u_2 = \delta_y \overline{y}, \quad u_3 = \delta_z \overline{z},$$

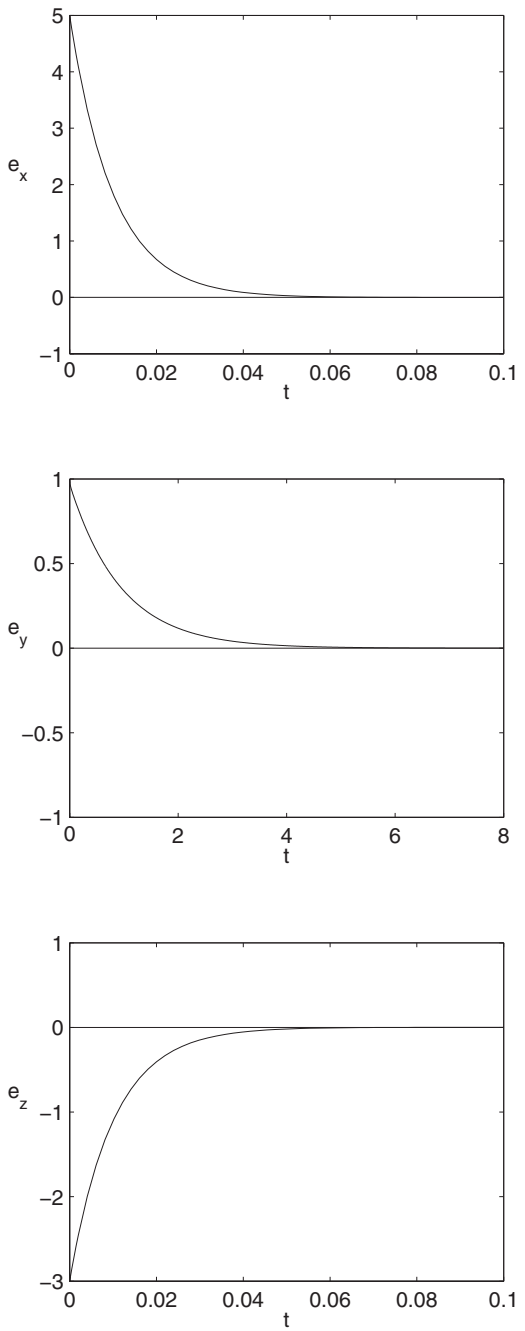

Fig. 9. Time history of the error system (27) for $a = b = c = 0.5$, $\tau_1 = \tau_2 = 100$, $r_1 = r_2 = s_1 = s_2 = 1$ with the control law given in Theorem 4-1, using the initial conditions, $x_d(0) = 20$, $y_d(0) = 5$, $z_d(0) = 5$ and $x_r(0) = 15$, $y_r(0) = 4$, $z_r(0) = 8$, when $\delta_x = 100$, $\delta_y = 1.05$ and $\delta_z = 100$.

where δ_x, δ_y and δ_z satisfy the conditions in Theorem 4, then the zero solution of the following error system:

$$\dot{\overline{x}} = \overline{y} - \frac{\tau_2}{\pi} \sum_{j=-r_2}^{s_2} f'_{2j}(\eta_{2j})\overline{y} - u_1(\overline{x}, \overline{y}, \overline{z}),$$

$$\dot{\overline{y}} = \overline{z} - u_2(\overline{x}, \overline{y}, \overline{z}),$$

$$\dot{\overline{z}} = -a\overline{x} - b\overline{y} - c\overline{z} + \frac{a\tau_1}{\pi} \sum_{j=-r_1}^{s_1} f'_{1j}(\eta_{1j})\overline{x} + \frac{b\tau_2}{\pi} \sum_{j=-r_2}^{s_2} f'_{2j}(\eta_{2j})\overline{y} - u_3(\overline{x}, \overline{y}, \overline{z}), \tag{31}$$

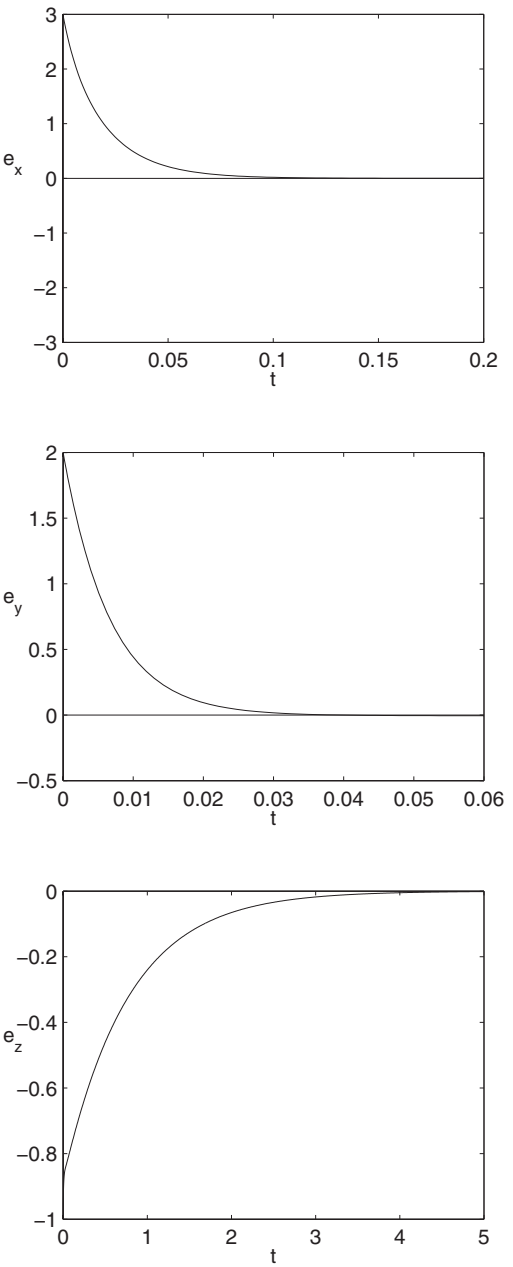

Fig. 10. Time history of the error system (27) for $a = b = c = 0.5$, $\tau_1 = \tau_2 = 100$, $r_1 = r_2 = s_1 = s_2 = 1$ with the control law given in Theorem 4-2, using the initial conditions, $x_d(0) = 15$, $y_d(0) = 1$, $z_d(0) = 5$ and $x_r(0) = 12$, $y_r(0) = -1$, $z_r(0) = 6$, when $\delta_x = 50$, $\delta_y = 150$ and $\delta_z = 0.8$.

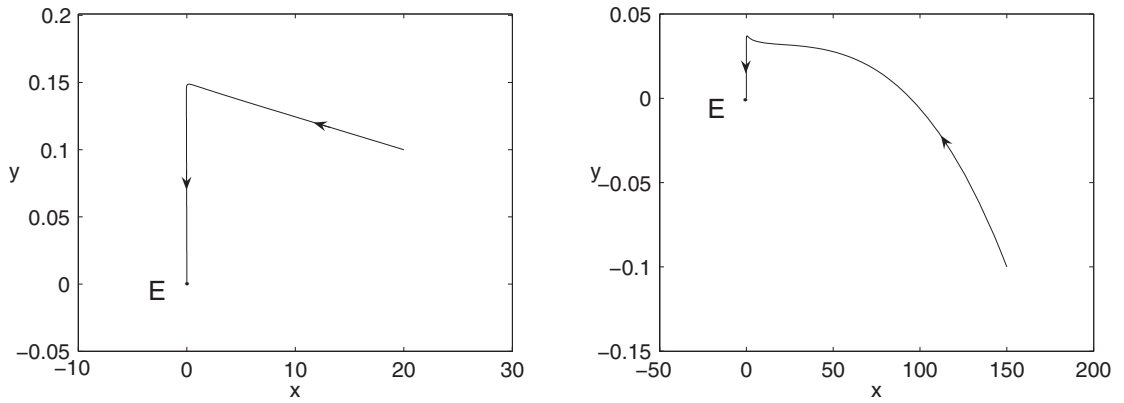

(a) (b)

Fig. 11. Trajectory of a 2-D-4 × 4-scroll chaotic attractor for system (31) when $a = b = c = 0.5$, $\tau_1 = \tau_2 = 100$, $r_1 = r_2 = s_1 = s_2 = 1$: (a) with the control law given in Corollary 7.1-1 for $\delta_x = 100$, $\delta_y = 1.05$ and $\delta_z = 100$ convergent to the equilibrium point, $E : (0, 0, 0)$ and (b) with the control law given in Corollary 7.1-2 for $\delta_x = 50$, $\delta_y = 150$ and $\delta_z = 0.8$ convergent to the equilibrium point, $E : (0, 0, 0)$.

is globally exponentially stabilized, i.e. the equilibrium point $X^* = (x^*, y^*, z^*)$ is globally exponentially stabilized.

For Corollary 7.1, we show a numerical example with the values of δ_x, δ_y and δ_z chosen as the same with that for Figs. 9 and 10. The simulation results (see Fig. 11) show that solution curves of system (31) globally exponentially converge to the equilibrium point $(0, 0, 0)$ under the proposed controls.

Theorem 5. *In system (27), choose the control law*:

$$u_1 = \delta_x e_x, \quad u_2 = \delta_y e_y, \quad u_3 = \delta_z e_z.$$

If the following conditions

$$\delta_x > 1 + \frac{\tau_2}{2\pi}(s_2 + r_2 + 1) + \frac{\tau_1}{2\pi}(s_1 + r_1 + 1),$$

$$\delta_y > 1 + \frac{\tau_2}{2\pi}(s_2 + r_2 + 1) + \frac{b\tau_2}{2a\pi}(s_2 + r_2 + 1) + \frac{b}{2a},$$

and

$$\delta_z > a + \frac{b}{2} + \frac{a\tau_1}{2\pi}(r_1 + s_1 + 1) + \frac{b\tau_2}{2\pi}(r_2 + s_2 + 1) - c,$$

are satisfied, then the zero solution of (27) is globally exponentially stabilized, and so the two systems (25) and (26) are globally exponentially synchronized.

Proof. Construct the positive definite, radially unbounded Lyapunov function:

$$V = \frac{1}{2}\left(e_x^2 + e_y^2 + \frac{e_z^2}{a}\right).$$

Then, we have

$$\begin{aligned}\left.\frac{dV}{dt}\right|_{(27)} &\le -\delta_x e_x^2 + e_x e_y + \frac{\tau_2}{\pi}(s_2 + r_2 + 1)|e_x||e_y| + e_y e_z - \delta_y e_y^2 - e_x e_z - \frac{b}{a}e_y e_z \\ &\quad - \frac{c}{a}e_z^2 - \frac{\delta_z e_z^2}{a} + \frac{\tau_1}{\pi}(s_1 + r_1 + 1)|e_x||e_z| + \frac{b\tau_2}{a\pi}(s_2 + r_2 + 1)|e_y||e_z| \\ &\le \begin{pmatrix}|e_x|\\|e_y|\\|e_z|\end{pmatrix}^T A_5 \begin{pmatrix}|e_x|\\|e_y|\\|e_z|\end{pmatrix},\end{aligned}$$

where

$$A_5 := \begin{bmatrix} -\delta_x & \frac{1}{2}+\frac{\tau_2}{2\pi}(s_2+r_2+1) & \frac{1}{2}+\frac{\tau_1}{2\pi}(s_1+r_1+1) \\ \frac{1}{2}+\frac{\tau_2}{2\pi}(s_2+r_2+1) & -\delta_y & \frac{1}{2}+\frac{b}{2a}+\frac{b\tau_2}{2a\pi}(s_2+r_2+1) \\ \frac{1}{2}+\frac{\tau_1}{2\pi}(s_1+r_1+1) & \frac{1}{2}+\frac{b}{2a}+\frac{b\tau_2}{2a\pi}(r_2+s_2+1) & -\frac{c}{a}-\frac{\delta_z}{a} \end{bmatrix}.$$

From the given conditions we know that A_5 is negative definite. Similar to the proof of Theorem 2, it is easy to prove that

$$e_x^2(t)+e_y^2(t)+e_z^2(t) \leq \frac{V(X(t))}{\lambda_m(P)} \leq \frac{V(X(t_0))}{\lambda_m(P)} e^{\frac{\lambda_M(A_5)}{\lambda_M(P)}(t-t_0)}, \quad (32)$$

which implies that the conclusion of Theorem 5 holds. ■

Corollary 7.2. *For any given equilibrium point $X = X^*$ of system (25), when the conditions in Theorem 5 hold, the zero solution of system (31) is globally exponentially stable. Thus the equilibrium point $X = X^*$ of (25) is globally exponentially stabilized.*

8. Synchronization and Stabilization of 3-D-$m \times n \times l$-Grid-Scroll Chaotic Attractors

Next, consider 3-D chaotic attractors. The driving system can be written as

$$\begin{aligned}
\dot{x}_d &= y_d - \frac{\tau_2}{2}\left[(r_2-s_2)+\sum_{j=-r_2}^{s_2}\frac{2}{\pi}\tan^{-1}(y_d+j\tau_2)\right], \\
\dot{y}_d &= z_d - \frac{\tau_3}{2}\left[(r_3-s_3)+\sum_{j=-r_3}^{s_3}\frac{2}{\pi}\tan^{-1}(z_d+j\tau_3)\right], \\
\dot{z}_d &= -ax_d - by_d - cz_d \\
&\quad + \frac{a\tau_1}{2}\left[(r_1-s_1)+\sum_{j=-r_1}^{s_1}\frac{2}{\pi}\tan^{-1}(x_d+j\tau_1)\right] \\
&\quad + \frac{b\tau_2}{2}\left[(r_2-s_2)+\sum_{j=-r_2}^{s_2}\frac{2}{\pi}\tan^{-1}(y_d+j\tau_2)\right] \\
&\quad + \frac{c\tau_3}{2}\left[(r_3-s_3)+\sum_{j=-r_2}^{s_2}\frac{2}{\pi}\tan^{-1}(z_d+j\tau_3)\right],
\end{aligned} \quad (33)$$

and the corresponding driven system with control laws is given by

$$\begin{aligned}
\dot{x}_r &= y_r - \frac{\tau_2}{2}\left[(r_2-s_2)+\sum_{j=-r_2}^{s_2}\frac{2}{\pi}\tan^{-1}(y_r+j\tau_2)\right] \\
&\quad + u_1(e_x,e_y,e_z), \\
\dot{y}_r &= z_r - \frac{\tau_3}{2}\left[(r_3-s_3)+\sum_{j=-r_3}^{s_3}\frac{2}{\pi}\tan^{-1}(z_r+j\tau_3)\right] \\
&\quad + u_3(e_x,e_y,e_z), \\
\dot{z}_r &= -ax_r - by_r - cz_r \\
&\quad + \frac{a\tau_1}{2}\left[(r_1-s_1)+\sum_{j=-r_1}^{s_1}\frac{2}{\pi}\tan^{-1}(x_r+j\tau_1)\right] \\
&\quad + \frac{b\tau_2}{2}\left[(r_2-s_2)+\sum_{j=-r_2}^{s_2}\frac{2}{\pi}\tan^{-1}(y_r+j\tau_2)\right] \\
&\quad + \frac{c\tau_3}{2}\left[(r_3-s_3)+\sum_{j=-r_3}^{s_3}\frac{2}{\pi}\tan^{-1}(z_r+j\tau_3)\right] \\
&\quad + u_3(e_x,e_y,e_z).
\end{aligned} \quad (34)$$

Then, the error system is obtained as

$$\begin{aligned}
\dot{e}_x &= e_y - \frac{\tau_2}{\pi}\sum_{j=-r_2}^{s_2} f'_{2j}(\xi_{2j})e_y - u_1(e_x,e_y,e_z), \\
\dot{e}_y &= e_z - \frac{\tau_3}{\pi}\sum_{j=-r_3}^{s_3} f'_{3j}(\xi_{3j})e_z - u_2(e_x,e_y,e_z),
\end{aligned}$$

$$\dot{e}_z = -ae_x - be_y - ce_z + \frac{a\tau_1}{\pi}\sum_{j=-r_1}^{s_1} f'_{1j}(\xi_{1j})e_x + \frac{b\tau_2}{\pi}\sum_{j=-r_2}^{s_2} f'_{2j}(\xi_{2j})e_y + \frac{c\tau_3}{\pi}\sum_{j=-r_3}^{s_3} f'_{3j}(\xi_{3j})e_z - u_3(e_x, e_y, e_z), \tag{35}$$

where, $f'_{1j}(\xi_{1j})e_x = \tan^{-1}(x_d + j\tau_1) - \tan^{-1}(x_r + j\tau_1)$, $\min(x_r, x_d) < \xi_{1j} < \max(x_r, x_d)$, $f'_{2j}(\xi_{2j})e_y = \tan^{-1}(y_d + j\tau_2) - \tan^{-1}(y_r + j\tau_2), \min(y_r, y_d) < \xi_{2j} < \max(y_r, y_d)$, $f'_{3j}(\xi_{3j})e_z = \tan^{-1}(z_d + j\tau_3) - \tan^{-1}(z_r + j\tau_3)$, and $\min(z_r, z_d) < \xi_{3j} < \max(z_r, z_d)$.

Theorem 6. *In system (34), choose the control law*:

$$u_1 = \delta_x e_x, \quad u_2 = \delta_y e_y, \quad u_3 = \delta_z e_z.$$

If for properly chosen $\delta_x \geq 0$, $\delta_y \geq 0$ *and* $\delta_z \geq 0$,

$$A_6 = \begin{bmatrix} -\delta_x & 1 + \frac{\tau_2}{\pi}(s_2 + r_2 + 1) & 0 \\ 0 & -\delta_y & 1 + \frac{\tau_3}{\pi}(s_3 + r_3 + 1) \\ \frac{a\tau_1}{\pi}(s_1 + r_1 + 1) + a & \frac{b\tau_2}{\pi}(s_2 + r_2 + 1) + b & -\delta_z - c + \frac{c\tau_3}{\pi}(s_3 + r_3 + 1) \end{bmatrix}$$

is a Hurwitz matrix, then the zero solution of (35) is globally exponentially stable. Thus, systems (33) and (34) are globally exponentially synchronized.

Proof. Construct the positive definite, radially unbounded vector Lyapunov function:

$$V = (|e_x|, |e_y|, |e_z|)^T.$$

We have

$$D^+V|_{(35)} = \begin{pmatrix} D^+|e_x| \\ D^+|e_y| \\ D^+|e_z| \end{pmatrix} \leq \begin{bmatrix} -\delta_x & 1 + \frac{\tau_2}{\pi}(s_2 + r_2 + 1) & 0 \\ 0 & -\delta_y & 1 + \frac{\tau_3}{\pi}(s_3 + r_3 + 1) \\ \frac{a\tau_1}{\pi}(s_1 + r_1 + 1) + a & \frac{b\tau_2}{\pi}(s_2 + r_2 + 1) + b & -\delta_z - c + \frac{c\tau_3}{\pi}(s_3 + r_3 + 1) \end{bmatrix} \begin{pmatrix} |e_x| \\ |e_y| \\ |e_z| \end{pmatrix}$$

$$:= A_6 \begin{pmatrix} |e_x| \\ |e_y| \\ |e_z| \end{pmatrix}. \tag{36}$$

Consider the comparison equation of (36), given by

$$\begin{pmatrix} \dot{\eta}_x \\ \dot{\eta}_y \\ \dot{\eta}_z \end{pmatrix} = \begin{bmatrix} -\delta_x & 1 + \frac{\tau_2}{\pi}(s_2 + r_2 + 1) & 0 \\ 0 & -\delta_y & 1 + \frac{\tau_3}{\pi}(s_3 + r_3 + 1) \\ \frac{a\tau_1}{\pi}(s_1 + r_1 + 1) + a & \frac{b\tau_2}{\pi}(s_2 + r_2 + 1) + b & -\delta_z - c + \frac{c\tau_3}{\pi}(s_3 + r_3 + 1) \end{bmatrix} \begin{pmatrix} \eta_x \\ \eta_y \\ \eta_z \end{pmatrix}$$

$$:= A_6 \begin{pmatrix} \eta_x \\ \eta_y \\ \eta_z \end{pmatrix}. \tag{37}$$

Since A_6 is a Hurwitz matrix, there exist constants $\alpha_6 > 0$ and $M_6 \geq 1$ satisfying

$$\begin{aligned}&\|(|e_x|, |e_y|, |e_z|)^T\| \\ &\quad \leq \|(\eta_x, \eta_y, \eta_z)^T\| \\ &\quad \leq M_6 e^{-\alpha_6(t-t_0)} \|(\eta_x(t_0), \eta_y(t_0), \eta_z(t_0))^T\|.\end{aligned}$$

The proof is complete. ■

To show the applicability of Theorem 6, we present a numerical example with $\delta_x = 165$, $\delta_y = 130$ and $\delta_z = 440$, satisfying the conditions in Theorem 6. It can be seen from Fig. 12 that under the proposed control law, the zero solution of system (35) is globally exponentially stabilized and thus systems (33) and (34) are globally exponentially synchronized.

Theorem 7. *In system (34), choose the same control law as used in Theorem 6. If*

$$A_7 = \begin{bmatrix} -\delta_x & \frac{1}{2} + \frac{\tau_2}{2\pi}(s_2 + r_2 + 1) & \frac{1}{2} + \frac{\tau_1}{2\pi}(s_1 + r_1 + 1) \\ \frac{1}{2} + \frac{\tau_2}{2\pi}(s_2 + r_2 + 1) & -\delta_y & \frac{a+b}{2a} + \frac{\tau_3}{2\pi}(s_3 + r_3 + 1) + \frac{b\tau_2}{2a\pi}(s_2 + r_2 + 1) \\ \frac{1}{2} + \frac{\tau_1}{2\pi}(s_1 + r_1 + 1) & \frac{a+b}{2a} + \frac{\tau_3}{2\pi}(s_3 + r_3 + 1) + \frac{b\tau_2}{2a\pi}(s_2 + r_2 + 1) & -\frac{c}{a} + \frac{c\tau_3}{a\pi}(s_3 + r_3 + 1) - \frac{\delta_z}{a} \end{bmatrix}$$

is a Hurwitz matrix, then the zero solution of system (35) is globally exponentially stable. Thus, systems (33) and (34) are globally exponentially synchronized.

Proof. We again use the Lyapunov function:

$$V = \frac{1}{2}\left(e_x^2 + e_y^2 + \frac{e_z^2}{a}\right),$$

and then we have

$$\begin{aligned}\left.\frac{dV}{dt}\right|_{(35)} &\leq |e_x e_y| + \frac{\tau_2}{\pi}(s_2 + r_2 + 1)|e_x e_y| - \delta_x e_x^2 + |e_y e_z| + \frac{\tau_3}{\pi}(s_3 + r_3 + 1)|e_y e_z| \\ &\quad - \delta_y e_y^2 + |e_x e_z| + \frac{b}{a}|e_y e_z| - \frac{c}{a}e_z^2 + \frac{\tau_1}{\pi}(s_1 + r_1 + 1)|e_x e_z| \\ &\quad + \frac{b\tau_2}{a\pi}(s_2 + r_2 + 1)|e_y e_z| + \frac{c\tau_3}{a\pi}(s_3 + r_3 + 1)e_z^2 - \frac{1}{a}\delta_z e_z^2 \\ &:= \begin{pmatrix} |e_x| \\ |e_y| \\ |e_z| \end{pmatrix}^T A_7 \begin{pmatrix} |e_x| \\ |e_y| \\ |e_z| \end{pmatrix}, \end{aligned} \tag{38}$$

from which the following estimation is obtained:

$$\begin{aligned}&e_x^2(t) + e_y^2(t) + e_z^2(t) \\ &\quad \leq \frac{V(X(t))}{\lambda_m(P)} \leq \frac{V(X(t_0))}{\lambda_m(P)} e^{\frac{\lambda_M(A_7)}{\lambda_M(P)}(t-t_0)},\end{aligned}$$

where the definitions of $\lambda_M(P)$, $\lambda_m(P)$ and $\lambda_M(A_7)$ are similar to those used in Theorem 2. Thus, the conclusion is true. ■

Corollary 8.1. *If the conditions given in Theorems 6 and 7 hold, then the zero solution of the following error system*:

$$\dot{\overline{x}} = -\delta_x \overline{x} + \overline{y} - \frac{\tau_2}{\pi}\sum_{j=-r_2}^{s_2} f'_{2j}(\eta_{2j})\overline{y},$$

$$\dot{\overline{y}} = -\delta_y \overline{y} - \frac{\tau_3}{\pi}\sum_{j=-r_3}^{s_3} f'_{3j}(\eta_{3j})\overline{z},$$

$$\dot{\overline{z}} = -(\delta_z + c)\overline{z} - a\overline{x} - b\overline{y} + \frac{a\tau_1}{\pi}\sum_{j=-r_1}^{s_1} f'_{1j}(\eta_{1j})\overline{x}$$

$$+\frac{b\tau_2}{\pi}\sum_{j=-r_2}^{s_2} f'_{2j}(\eta_{2j})\overline{y}+\frac{c\tau_3}{\pi}\sum_{j=-r_3}^{s_3} f'_{3j}(\eta_{3j})\overline{z}, \tag{39}$$

is globally exponentially stable. Thus the equilibrium point $X = X^*$ is globally exponentially stabilized.

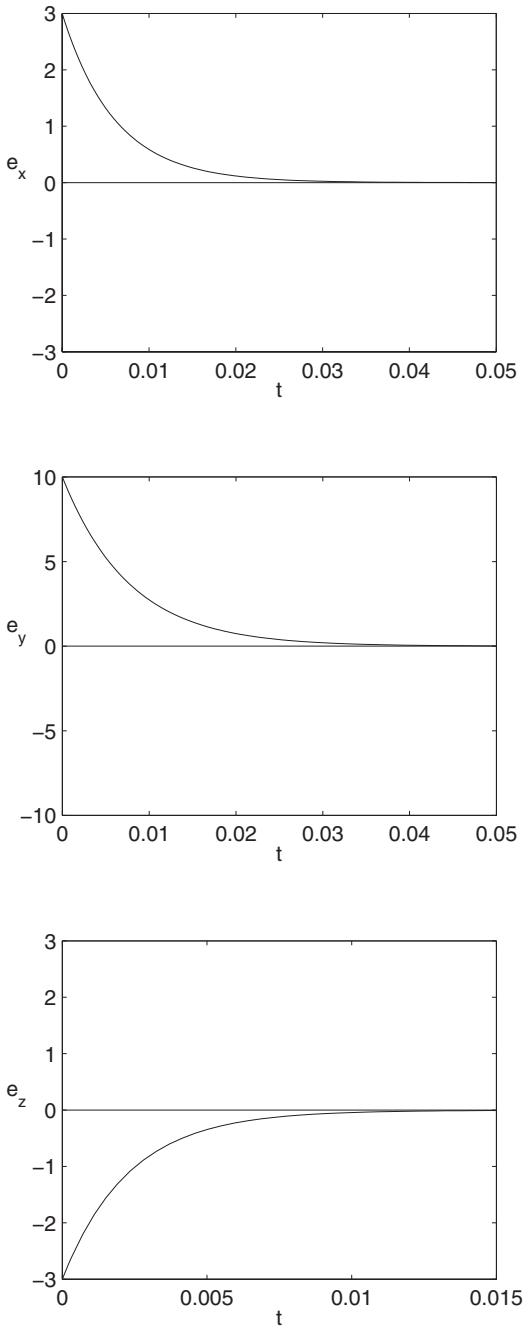

Fig. 12. Time history of the error system (35) for $a = b = c = 0.8$, $\tau_1 = 160$, $\tau_2 = 100$, $\tau_3 = 80$, $r_1 = r_2 = s_1 = s_2 = 2$ with the control law given in Theorem 6, using the initial conditions, $x_d(0) = 11$, $y_d(0) = 12$, $z_d(0) = 1$ and $x_r(0) = 8$, $y_r(0) = 2$, $z_r(0) = 4$, when $\delta_x = 165$, $\delta_y = 130$ and $\delta_z = 440$.

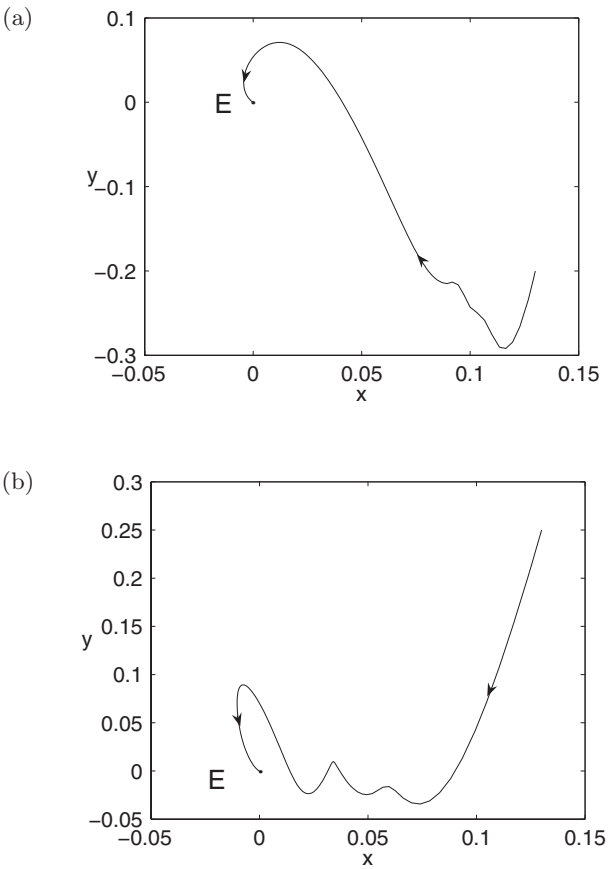

Fig. 13. Trajectory of a 3-D-$6\times6\times6$-scroll chaotic attractor for system (39) when $a = b = c = 0.8$, $\tau_1 = 160$, $\tau_2 = 100$, $\tau_3 = 80$, and $r_1 = r_2 = r_3 = s_1 = s_2 = s_3 = 2$ with the control law given in Corollary 8.1: (a) for $\delta_x = 165$, $\delta_y = 130$ and $\delta_z = 440$ convergent to the equilibrium point, $E : (0, 0, 0)$ and (b) for $\delta_x = 210$, $\delta_y = 300$ and $\delta_z = 250$ convergent to the equilibrium point, $E : (0, 0, 0)$.

To end this section, we present a numerical example to demonstrate the applicability of Corollary 8.1. The simulations are shown in Fig. 13. For the results shown in Fig. 13(a), we choose $\delta_x = 165$, $\delta_y = 130$ and $\delta_z = 440$, satisfying one condition of Corollary 8.1 (the condition of Theorem 6); while for that in Fig. 13(b), we choose $\delta_x = 210$, $\delta_y = 300$ and $\delta_z = 250$, satisfying the other condition of Corollary 8.1 (the condition of Theorem 7). These two figures indicate that under the proposed controls, the solution orbits of system (39) globally exponentially converge to the equilibrium point $(0, 0, 0)$.

9. Fractional Order Multi-Scroll Chaotic Attractors

In this section, we investigate fractional order multi-scroll chaotic attractors. We first introduce the

definition of fractional derivative. Since this definition is not unique, we adopt the most commonly used one in this article, which is given by

$$D^{\alpha}y(t) = J^{m-\alpha}\frac{d^m}{dt^m}y(t), \tag{40}$$

where $\frac{d^m}{dt^m}y(t)$ is the general definition of mth-order derivative, $\alpha > 0$, and $m = \lceil\alpha\rceil = \min\{m \in \mathbb{R} \,|\, m \geq \alpha\}$. Here, the β-order Riemann–Liouville integral operator, J^{β}, is given by

$$J^{\beta}z(t) = \frac{\int_0^t (t-\tau)^{\beta-1}z(\tau)d\tau}{\Gamma(\beta)}, \quad \text{for } \beta > 0.$$

In the previous sections, we have investigated the three-dimensional integer order differential systems in the form of

$$\begin{aligned} Dx(t) &= f_1(x, y, z), \\ Dy(t) &= f_2(x, y, z), \\ Dz(t) &= f_3(x, y, z). \end{aligned} \tag{41}$$

The corresponding fractional order system can be written as

$$\begin{aligned} D^{\alpha_1}x(t) &= f_1(x, y, z), \\ D^{\alpha_2}y(t) &= f_2(x, y, z), \\ D^{\alpha_3}x(t) &= f_3(x, y, z), \end{aligned} \tag{42}$$

where $\alpha_i \in (0, 1)$, $i = 1, 2, 3$, are the orders of the fractional order differential equations.

9.1. *Design of fractional order 1-D-n-scroll chaotic attractors*

We first consider the design of 1-D chaos generator using fractional order differential system. The corresponding fractional order system of (3) is given by

$$\begin{aligned} D^{\alpha_1}x(t) &= y, \\ D^{\alpha_2}y(t) &= z, \\ D^{\alpha_3}x(t) &= -ax - by - cz \\ &\quad + ad\left[(r-s) + \frac{2}{\pi}\sum_{j=-r}^{s}\tan^{-1}(x + j\tau)\right], \end{aligned} \tag{43}$$

where $\alpha_i \in (0, 1)$, $i = 1, 2, 3$, a, b, c and d take positive real values. As discussed in the previous sections, the maximum number of chaotic scrolls is determined by the non-negative integers s and r.

Next, we use numerical simulations to verify the existence of the fractional order 1-D-n-scroll chaotic attractors. Our first example is to create a fractional order double-scroll chaotic attractor. Thus, we let $r = s = 0$. All the other parameters are chosen as follows:

$$a = b = c = 0.7, \quad d = 65, \quad r = s = 0,$$
$$\alpha_1 = 0.98, \quad \alpha_2 = 0.97, \quad \alpha_3 = 0.98.$$

As shown in Fig. 14, with the above chosen parameter values, the fractional order system (43) exhibits double-scroll chaotic behavior.

A 1-D-6-scroll chaotic attractor can be created by choosing $r = s = 2$. For example, by taking

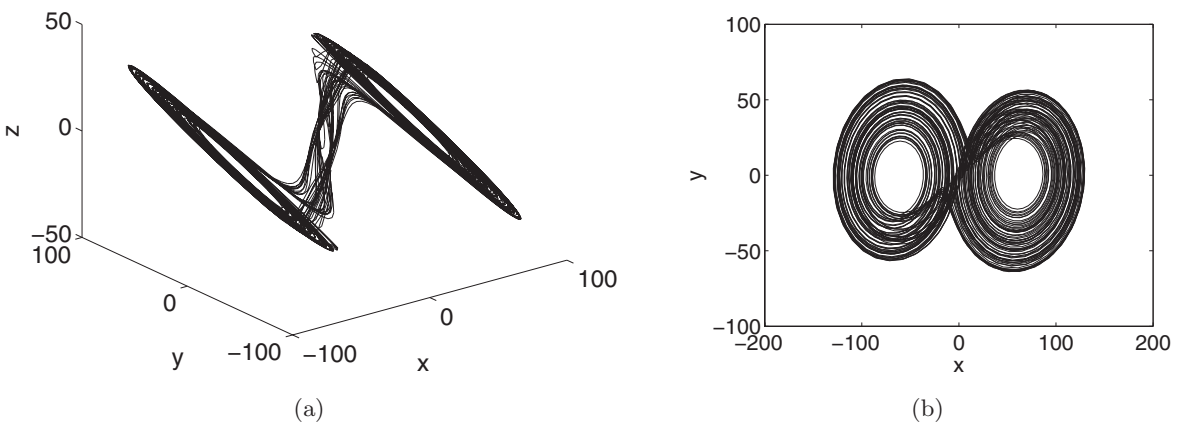

(a) (b)

Fig. 14. Simulated phase portrait of a fractional order double-scroll chaotic attractor for system (43) when $a = b = c = 0.7$, $d = 65$, $r = s = 0$, $\alpha_1 = 0.98$, $\alpha_2 = 0.97$, $\alpha_3 = 0.98$: (a) in the x–y–z space and (b) projected on the x–y plane.

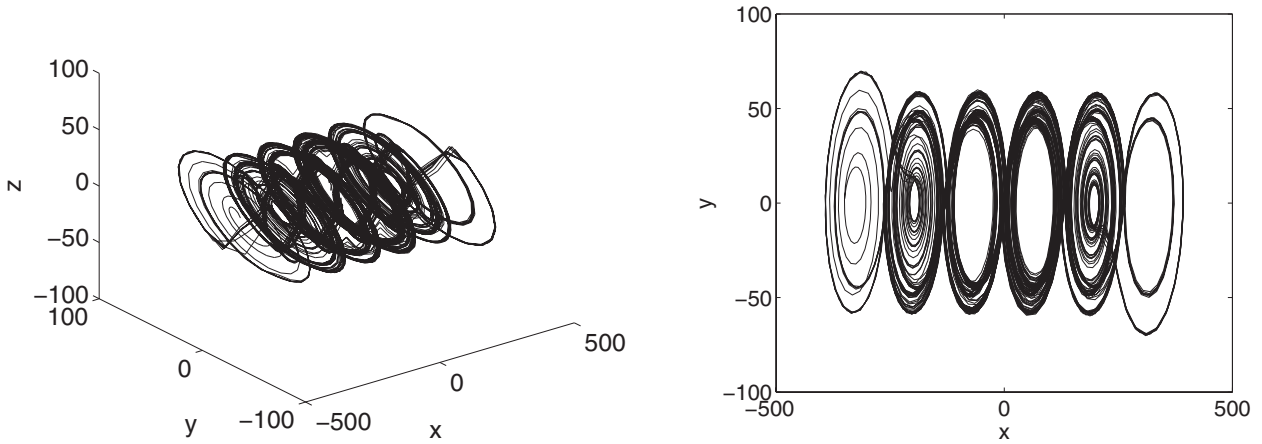

Fig. 15. Simulated phase portrait of a fractional order double-scroll chaotic attractor for system (43) when $a = b = c = 0.7$, $d = 65$, $r = s = 2$, $\alpha_1 = 0.98$, $\alpha_2 = 0.99$, $\alpha_3 = 0.99$: (a) in the x–y–z space and (b) projected on the x–y plane.

$a = b = c = 0.7$, $d = 65$, $\alpha_1 = 0.98$, $\alpha_2 = 0.99$, $\alpha_3 = 0.99$, for system (43), we obtain a one-dimensional chaotic attractor with six scrolls, as shown in Fig. 15.

9.2. *Design of fractional order 2-D-$m \times n$-grid-scroll chaotic attractors*

In order to create a fractional order chaotic attractor with 2-directional $m \times n$-grid scrolls, we apply the fractional derivative to (6) and obtain the following fractional order differential system:

$$\begin{aligned}
&D^{\alpha_1}x(t)\\
&\quad = y - \frac{\tau_2}{2}\left[(r_2 - s_2) + \sum_{j=-r_2}^{s_2}\frac{2}{\pi}\tan^{-1}(y + j\tau_2)\right],\\
&D^{\alpha_2}y(t) = z,\\
&D^{\alpha_3}x(t)\\
&\quad = -ax - by - cz\\
&\qquad + a\frac{\tau_1}{2}\left[(r_1 - s_1) + \sum_{j=-r_1}^{s_1}\frac{2}{\pi}\tan^{-1}(x + j\tau_1)\right]\\
&\qquad + b\frac{\tau_2}{2}\left[(r_2 - s_2) + \frac{2}{\pi}\sum_{j=-r_2}^{s_2}\tan^{-1}(y + j\tau_2)\right],
\end{aligned} \tag{44}$$

where parameters a, b, c, τ_1, τ_2 and τ_3 are all taken positive, and the number of scrolls that system (44) can generate depends on non-negative integers r_1 and r_2. As discussed previously $m = r_1 + s_1 + 2$ and $n = r_2 + s_2 + 2$. In (44), $\alpha_i \in (0, 1)$, $i = 1, 2, 3$, are the orders of the fractional order differential equations.

System (44) exhibits rich dynamical phenomena with properly chosen parameter values. For example, if we let

$$\begin{aligned}
a = b = c = 0.5,\\
\tau_1 = \tau_2 = 100,\\
r_1 = r_2 = s_1 = s_2 = 1,\\
\alpha_1 = \alpha_2 = \alpha_3 = 0.99,
\end{aligned}$$

as shown in Fig. 16, a 2-D-4×4-scroll chaotic attractor is generated.

9.3. *Design of fractional order 3-D-$m \times n \times l$-grid-scroll chaotic attractors*

The fractional order 3-D-$m \times n \times l$-grid-scroll chaotic attractor generator can be similarly obtained by applying fractional derivative to system (7), yielding the system,

$$\begin{aligned}
&D^{\alpha_1}x(t)\\
&\quad = y - \frac{\tau_2}{2}\left[(r_2 - s_2) + \sum_{j=-r_2}^{s_2}\frac{2}{\pi}\tan^{-1}(y + j\tau_2)\right],
\end{aligned}$$

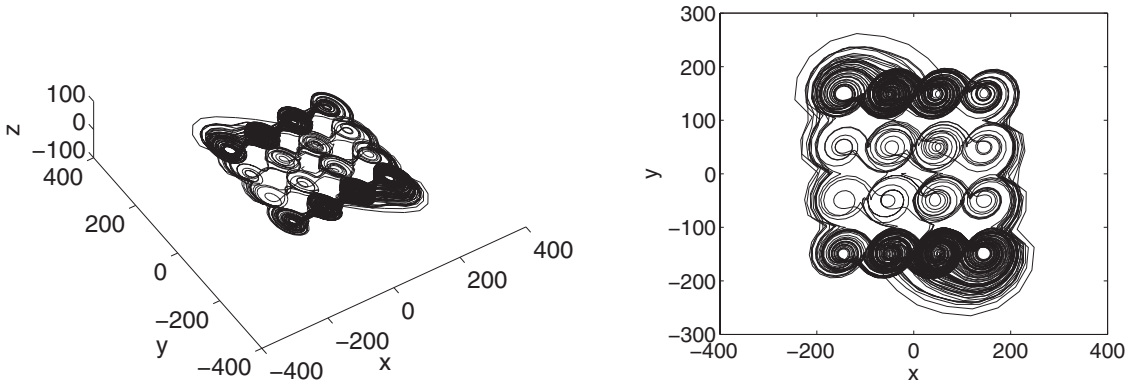

(a) (b)

Fig. 16. Simulated phase portrait of a 2-D-4 × 4-scroll chaotic attractor for system (44) when $a = b = c = 0.5$, $\tau_1 = \tau_2 = 100$, $r_1 = r_2 = s_1 = s_2 = 1$, $\alpha_1 = \alpha_2 = \alpha_3 = 0.99$: (a) in the x–y–z space and (b) projected on the x–y plane.

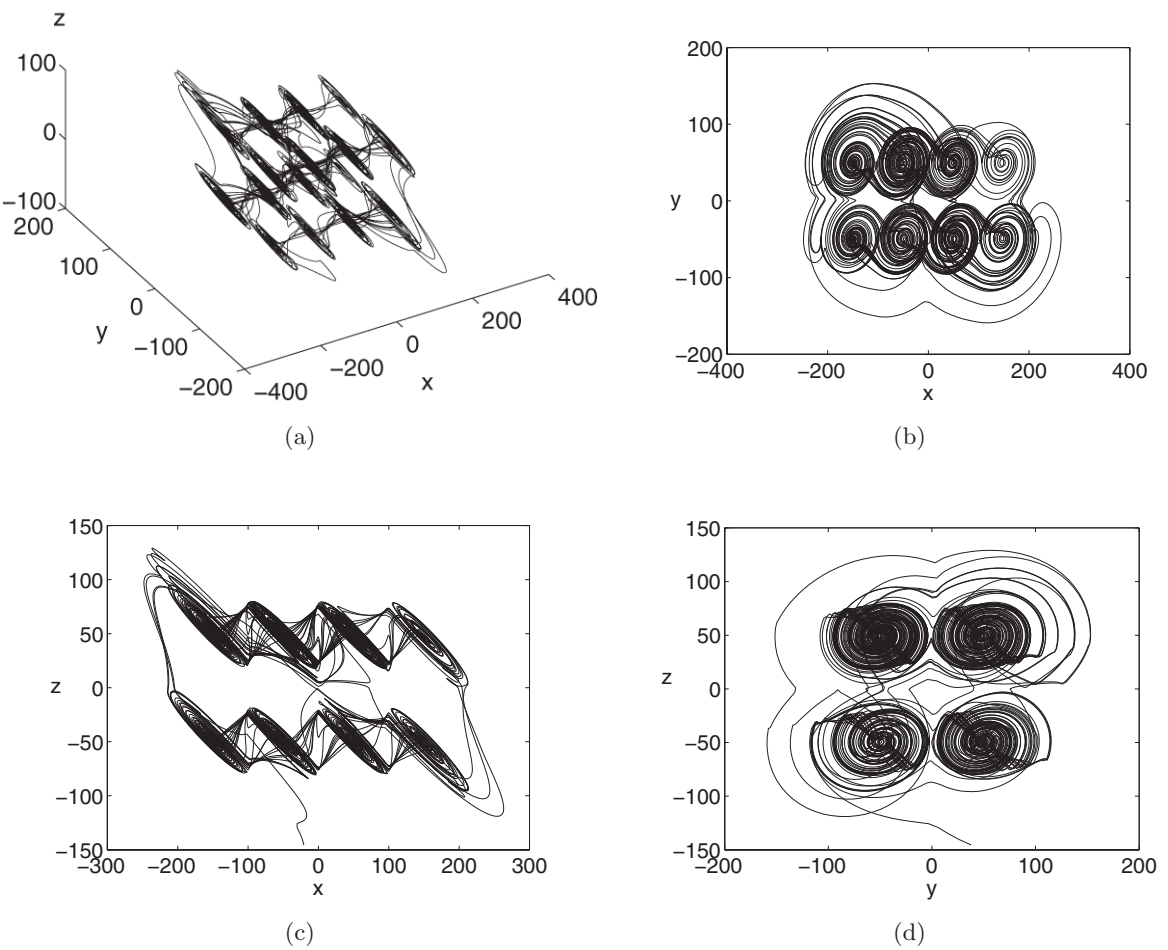

(a) (b)

(c) (d)

Fig. 17. Simulated phase portrait of a 3-D-4 × 2 × 2-grid-scroll fractional order chaotic attractor for system (45) when $a = b = c = 0.5$, $\tau_1 = \tau_2 = \tau_3 = 100$, $r_1 = s_1 = 1$, $r_2 = s_2 = 0$, $r_3 = s_3 = 0$, $\alpha_1 = 0.99$, $\alpha_2 = 0.99$, $\alpha_3 = 0.998$: (a) in the x–y–z space, (b) projected on the x–y plane, (c) projected on the x–z plane and (d) projected on the y–z plane.

$$
\begin{aligned}
&D^{\alpha_2} y(t) \\
&\quad = z - \frac{\tau_3}{2}\left[(r_3 - s_3) + \sum_{j=-r_3}^{s_3} \frac{2}{\pi}\tan^{-1}(z + j\tau_3)\right], \\
&D^{\alpha_3} z(t) \\
&\quad = -ax - by - cz \\
&\qquad + a\frac{\tau_1}{2}\left[(r_1 - s_1) + \sum_{j=-r_1}^{s_1} \frac{2}{\pi}\tan^{-1}(x + j\tau_1)\right] \\
&\qquad + b\frac{\tau_2}{2}\left[(r_2 - s_2) + \sum_{j=-r_2}^{s_2} \frac{2}{\pi}\tan^{-1}(y + j\tau_2)\right] \\
&\qquad + c\frac{\tau_3}{2}\left[(r_3 - s_3) + \sum_{j=-r_3}^{s_3} \frac{2}{\pi}\tan^{-1}(z + j\tau_3)\right],
\end{aligned} \tag{45}
$$

where a, b, c, τ_1, τ_2 and τ_3 are positive real numbers, $r_1, r_2, r_3, s_1, s_2, s_3$ are non-negative integers, and $\alpha_i \in (0, 1)$, $i = 1, 2, 3$, are the orders of the fractional order differential equations. The maximum number of grid chaotic scrolls that system (45) can generate is $(r_1 + s_1 + 2) \times (r_2 + s_2 + 2) \times (r_3 + s_3 + 2)$, i.e. $m = r_1 + s_1 + 2$, $n = r_2 + s_2 + 2$ and $l = r_3 + s_3 + 2$.

Next, we investigate the chaotic behaviors of system (45) using numerical simulations. By choosing

$$
\begin{gathered}
a = b = c = 0.5, \quad \tau_1 = \tau_2 = \tau_3 = 100, \\
r_1 = s_1 = 1, \quad r_2 = s_2 = 0, \quad r_3 = s_3 = 0, \\
\alpha_1 = 0.99, \quad \alpha_2 = 0.99, \quad \alpha_3 = 0.998,
\end{gathered}
$$

we obtain a chaotic trajectory from the fractional order system (45), with 3-D-4 × 2 × 2-grid scrolls (see Fig. 17).

10. Synchronization and Stabilization of Fractional Order Multi-Scroll Chaotic Attractors

In this section, we consider synchronization and stabilization of the fractional order multi-scroll chaotic attractors by constructing simple control laws. In Secs. 6–8, the integer order multi-scroll chaotic attractors have been synchronized and stabilized using feedback control strategies. Here, we extend the feedback control method to study synchronization and stabilization of the fractional order multi-scroll chaotic attractors which are obtained in Sec. 9.

In general, a three-dimensional fractional order system has the form

$$
\begin{aligned}
D^{\alpha_1} x(t) &= f_1(x, y, z), \\
D^{\alpha_2} y(t) &= f_2(x, y, z), \\
D^{\alpha_3} x(t) &= f_3(x, y, z),
\end{aligned} \tag{46}
$$

where $\alpha_i \in (0, 1)$, for $i = 1, 2, 3$. We can solve the following equations:

$$
\begin{aligned}
f_1(x, y, z) &= 0, \\
f_2(x, y, z) &= 0, \\
f_3(x, y, z) &= 0,
\end{aligned} \tag{47}
$$

to obtain the equilibrium point, denoted as (x^*, y^*, z^*). To study the stability of system (46), we evaluate its corresponding Jacobian matrix at equilibrium point (x^*, y^*, z^*) to obtain

$$
M = \left.\begin{pmatrix}
\dfrac{\partial f_1}{\partial x} & \dfrac{\partial f_1}{\partial y} & \dfrac{\partial f_1}{\partial z} \\
\dfrac{\partial f_2}{\partial x} & \dfrac{\partial f_2}{\partial y} & \dfrac{\partial f_2}{\partial z} \\
\dfrac{\partial f_3}{\partial x} & \dfrac{\partial f_3}{\partial y} & \dfrac{\partial f_3}{\partial z}
\end{pmatrix}\right|_{(x=x^*, y=y^*, z=z^*)}.
$$

Theorem 8 [Matignon, 1996; Ahmed *et al.*, 2007]. *If the eigenvalues of the Jacobian matrix M satisfy*

$$
\arg(\lambda) \geq \frac{\pi\theta}{2}, \tag{48}
$$

where $\theta = \max(\alpha_1, \alpha_2, \alpha_3)$, then the equilibrium point (x^*, y^*, z^*) is asymptotically stable.

For a linear fractional order differential system, its stability region is bounded by a cone in the right-half s-plane with an angle of $\pm\frac{\pi\theta}{2}$. The vertex of the cone is at the origin [Matignon, 1996]. The stability and instability regions of the fractional order system (46), with $\alpha_1 = \alpha_2 = \alpha_3 = \alpha$ in the complex plane are shown in Fig. 18.

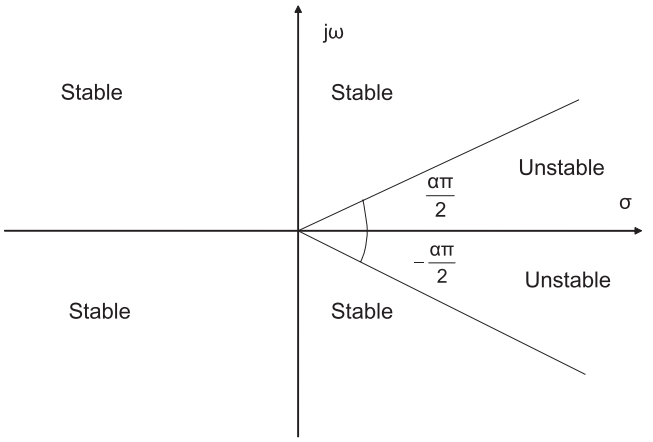

Fig. 18. Stability region in the complex plane for fractional order system (46) when $\alpha_1 = \alpha_2 = \alpha_3 = \alpha$.

10.1. *Synchronization and stabilization of fractional order 1-D-n-scroll chaotic attractors*

In this section, we construct simple feedback control laws to realize the synchronization and stabilization of the fractional order 1-D-n-scroll chaotic attractors. We first consider the synchronization of two such systems. One of the systems serves as the driving system (transmitter), which is given by

$$\begin{aligned} &D^{\alpha_1} x_d(t) = y_d, \\ &D^{\alpha_2} y_d(t) = z_d, \\ &D^{\alpha_3} z_d(t) \\ &\quad = -a x_d - b y_d - c z_d \\ &\qquad + ad\left[(r-s) + \frac{2}{\pi}\sum_{j=-r}^{s} \tan^{-1}(x_d + j\tau)\right], \end{aligned} \tag{49}$$

with the corresponding driven system obtained as

$$\begin{aligned} &D^{\alpha_1} x_r(t) = y_r + u_1(x_d - x_r, y_d - y_r, z_d - z_r), \\ &D^{\alpha_2} y_r(t) = z_r + u_2(x_d - x_r, y_d - y_r, z_d - z_r), \\ &D^{\alpha_3} z_r(t) \\ &\quad = -a x_r - b y_r - c z_r \\ &\qquad + ad\left[(r-s) + \frac{2}{\pi}\sum_{j=-r}^{s} \tan^{-1}(x_r + j\tau)\right] \\ &\qquad + u_3(x_d - x_r, y_d - y_r, z_d - z_r), \end{aligned} \tag{50}$$

where u_i's are the controls to be designed.

The difference between the driving system and the driven system is defined by $e_x = x_d - x_r$, $e_y = y_d - y_r$ and $e_z = z_d - z_r$. Thus, the error system is given by

$$\begin{aligned} &D^{\alpha_1} e_x = e_y - u_1(e_x, e_y, e_z), \\ &D^{\alpha_2} e_y = e_z - u_2(e_x, e_y, e_z), \\ &D^{\alpha_3} e_z = -a e_x - b e_y - c e_z \\ &\qquad + \sum_{j=-r}^{s} \frac{2ad}{\pi} f_j'(\xi_j) e_x - u_3(e_x, e_y, e_z). \end{aligned} \tag{51}$$

Theorem 9. *Applying the following simple linear feedback control law*:

$$u_1 = \delta_x e_x, \quad u_2 = \delta_y e_y, \quad u_3 = \delta_z e_z, \tag{52}$$

to system (51), if one of the following conditions holds:

(1) $\delta_x > 1, \quad \delta_y > 1,$

$$\delta_z > a + b - c + \frac{2ad}{\pi}(s + r + 1);$$

(2) $\delta_x > a + \frac{2ad}{\pi}(s + r + 1), \quad \delta_y > b + 1,$

$$\delta_z > 1 - c;$$

then the zero solution of (51) is stabilized, and as such the driving-driven system pairs (49) and (50) are synchronized.

Proof. Evaluating the Jacobian matrix of the error system (51) yields

$$J_{F1D} = \begin{bmatrix} -\delta_x & 1 & 0 \\ 0 & -\delta_y & 1 \\ -a + \dfrac{2ad}{\pi}\displaystyle\sum_{j=-r}^{s} f_j'(\xi_j) & -b & -c - \delta_z \end{bmatrix}. \tag{53}$$

Then, we apply the Gersgorin's Theorem to row sums. It is obvious that when condition (1) holds, all eigenvalues of J_{F1D} are located in the left half of the s-plane. Similarly, by applying the Gersgorin's Theorem to column sums, we can prove that when condition (2) holds, all eigenvalues of J_{F1D} are located in the left half of the s-plane. Since

$$\arg(\lambda) \geq \frac{\pi\theta}{2},$$

where $\theta = \max(\alpha_1, \alpha_2, \alpha_3)$, then according to Theorem 8, the zero solution of system (51) is stabilized and hence the driving system (49) and its corresponding driven system (50) are synchronized. ■

Next, we use numerical simulations to verify the effectiveness of the control laws in Theorem 9. As shown in Fig. 19, when $\delta_x = 4$, $\delta_y = 4$ and $\delta_z = 300$

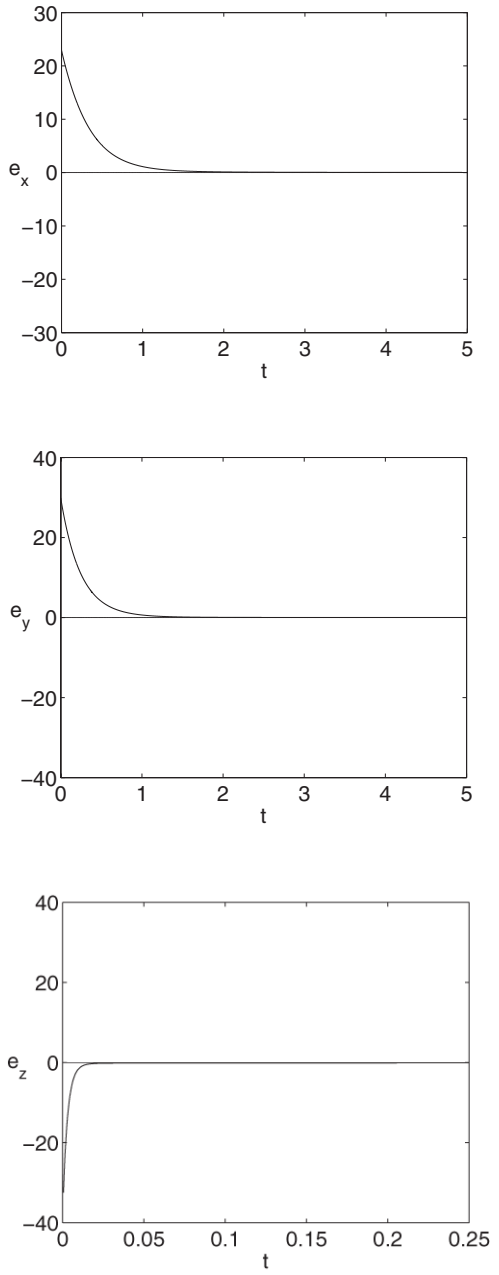

Fig. 19. Time history of the error system (51) for $a = b = c = 0.7$, $d = 65$, $r = s = 2$, $\alpha_1 = 0.98$, $\alpha_2 = \alpha_3 = 0.99$ with the control law given in Theorem 9, using the initial conditions, $x_d(0) = 26$, $y_d(0) = 32$, $z_d(0) = -30$ and $x_r(0) = 3$, $y_r(0) = 2$, $z_r(0) = 8$, when $\delta_x = 4$, $\delta_y = 4$ and $\delta_z = 300$.

(i.e. condition 1 of Theorem 9 is satisfied), the zero solution of the error system (51) is stabilized and thus its corresponding driving-driven system pair, (49) and (50), is synchronized.

Let $\overline{X} = X - X^* = (x - x^*, y - y^*, z - z^*)$, where $X^* = (x^*, y^*, z^*)$ is any equilibrium point of system (43). Then system (51) can be rewritten as

$$\begin{aligned} D^{\alpha_1}\overline{x} &= \overline{y} - u_1(\overline{x}, \overline{y}, \overline{z}), \\ D^{\alpha_2}\overline{y} &= \overline{z} - u_2(\overline{x}, \overline{y}, \overline{z}), \\ D^{\alpha_3}\overline{z} &= -a\overline{x} - b\overline{y} - c\overline{z} \\ &\quad + \sum_{j=-r}^{s} \frac{2ad}{\pi} f_j'(\eta_j)\overline{x} - u_3(\overline{x}, \overline{y}, \overline{z}). \end{aligned} \tag{54}$$

Corollary 10.1. *Apply the following feedback control law*:

$$u_1 = \delta_x \overline{x}, \quad u_2 = \delta_y \overline{y}, \quad u_3 = \delta_z \overline{z} \tag{55}$$

to system (54) with respect to any given equilibrium $X = X^*$, then either of the following conditions

(1) $\delta_x > 1, \quad \delta_y > 1,$

$$\delta_z > a + b - c + \frac{2ad}{\pi}(s + r + 1);$$

(2) $\delta_x > a + \dfrac{2ad}{\pi}(s + r + 1), \quad \delta_y > b + 1,$

$$\delta_z > 1 - c;$$

guarantees the stability of $X^* = (x^*, y^*, z^*)$.

To show the applicability of Corollary 10.1, we present a numerical example, for which we choose $\delta_x = 4$, $\delta_y = 4$ and $\delta_z = 300$, satisfying the first condition of Corollary 10.1. As indicated in Fig. 20, under the given control law, the trajectory of system (54) converges to the equilibrium point $(0, 0, 0)$.

10.2. *Synchronization and stabilization of fractional order 2-D-$m \times n$-grid-scroll chaotic attractors*

Next, we consider synchronization and stabilization of the fractional order 2-D-$m \times n$-grid-scroll chaotic attractors using simple feedback control laws. In order to synchronize two such chaotic systems, we let one of them be the driving system, which can be

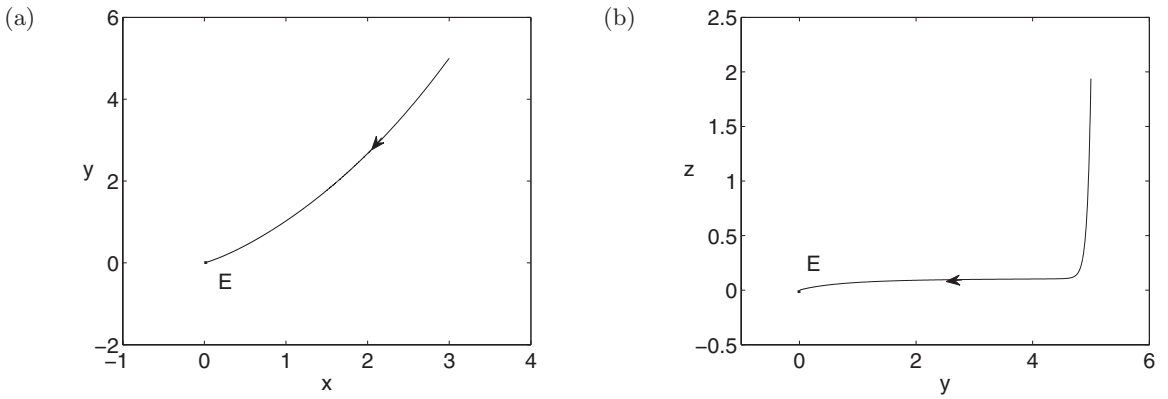

Fig. 20. Trajectory of a 1-D-6-scroll chaotic attractor for system (54) when $a = b = c = 0.7$, $d = 65$, $r = s = 2$, $\alpha_1 = 0.98$, $\alpha_2 = \alpha_3 = 0.99$ with the control law given in Corollary 10.1 for $\delta_x = 4$, $\delta_y = 4$ and $\delta_z = 300$, convergent to the equilibrium point, $E(0, 0, 0)$: (a) projected on the x–y plane and (b) projected on the y–z plane.

described as

$$\begin{aligned} D^{\alpha_1}x_d(t) &= y_d - \frac{\tau_2}{2}\left[(r_2 - s_2) + \sum_{j=-r_2}^{s_2}\frac{2}{\pi}\tan^{-1}(y_d + j\tau_2)\right], \quad D^{\alpha_2}y_d(t) = z_d, \\ D^{\alpha_3}z_d(t) &= -ax_d - by_d - cz_d + \frac{a\tau_1}{2}\left[(r_1 - s_1) + \sum_{j=-r_1}^{s_1}\frac{2}{\pi}\tan^{-1}(x_d + j\tau_1)\right] \\ &\quad + \frac{b\tau_2}{2}\left[(r_2 - s_2) + \sum_{j=-r_2}^{s_2}\frac{2}{\pi}\tan^{-1}(y_d + j\tau_2)\right]. \end{aligned} \tag{56}$$

The corresponding driven system of (56) is then obtained as

$$\begin{aligned} D^{\alpha_1}x_r(t) &= y_r - \frac{\tau_2}{2}\left[(r_2 - s_2) + \sum_{j=-r_2}^{s_2}\frac{2}{\pi}\tan^{-1}(y_r + j\tau_2)\right] + u_1(e_x, e_y, e_z), \\ D^{\alpha_2}y_r(t) &= z_r + u_2(e_x, e_y, e_z), \\ D^{\alpha_3}z_r(t) &= -ax_r - by_r - cz_r + \frac{a\tau_1}{2}\left[(r_1 - s_1) + \sum_{j=-r_1}^{s_1}\frac{2}{\pi}\tan^{-1}(x_r + j\tau_1)\right] \\ &\quad + \frac{b\tau_2}{2}\left[(r_2 - s_2) + \sum_{j=-r_2}^{s_2}\frac{2}{\pi}\tan^{-1}(y_r + j\tau_2)\right] + u_3(e_x, e_y, e_z), \end{aligned} \tag{57}$$

where u_i's are the controls.

It follows from systems (56) and (57) that the error system is given by

$$\begin{aligned} D^{\alpha_1}e_x &= e_y - \frac{\tau_2}{\pi}\sum_{j=-r_2}^{s_2} f'_{2j}(\xi_{2j})e_y - u_1(e_x, e_y, e_z), \quad D^{\alpha_2}e_y = e_z - u_2(e_x, e_y, e_z), \\ D^{\alpha_3}e_z &= -ae_x - be_y - ce_z + \frac{a\tau_1}{\pi}\sum_{j=-r_1}^{s_1} f'_{1j}(\xi_{1j})e_x + \frac{b\tau_2}{\pi}\sum_{j=-r_2}^{s_2} f'_{2j}(\xi_{2j})e_y - u_3(e_x, e_y, e_z). \end{aligned} \tag{58}$$

Theorem 10. *If we apply the following simple linear feedback control law*:

$$u_1 = \delta_x e_x, \quad u_2 = \delta_y e_y, \quad u_3 = \delta_z e_z, \tag{59}$$

to system (*51*) *with one of the following conditions*,

(1) $\delta_x > 1 + \frac{\tau_2}{\pi}(s_2 + r_2 + 1)$,

$\delta_y > 1$,

$\delta_z > a + \frac{a\tau_1}{\pi}(s_1 + r_1 + 1) + b + \frac{b\tau_2}{\pi}(s_2 + r_2 + 1) - c$;

(2) $\delta_x > a + \frac{a\tau_1}{\pi}(s_1 + r_1 + 1)$,

$\delta_y > 1 + \frac{\tau_2}{\pi}(s_2 + r_2 + 1) + b + \frac{b\tau_2}{\pi}(s_2 + r_2 + 1)$,

$\delta_z > 1 - c$;

to hold, then the zero solution of (*58*) *is stabilized, and hence the driving system* (*56*) *and the driven system* (*57*) *are synchronized.*

Proof. The proof is similar to that for Theorem 9, and is thus omitted. ■

Now, we verify the control laws given in Theorem 10 numerically. If we take $\delta_x = 90$, $\delta_y = 180$ and $\delta_z = 1$, the second condition of Theorem 10 is satisfied. Using the proposed control law, the zero solution of system (58) is stabilized, as shown in Fig. 21, indicating that the driving system (56) and its corresponding driven system (57) are synchronized.

Corollary 10.2. *For any given equilibrium* $X = X^*$, *with the following feedback control law*,

$$u_1 = \delta_x \overline{x}, \quad u_2 = \delta_y \overline{y}, \quad u_3 = \delta_z \overline{z}, \tag{60}$$

applied to the following system:

$$\begin{aligned}
D^{\alpha_1}\overline{x} &= \overline{y} - \frac{\tau_2}{\pi}\sum_{j=-r_2}^{s_2} f'_{2j}(\eta_{2j})\overline{y} - u_1(\overline{x},\overline{y},\overline{z}),\\
D^{\alpha_2}\overline{y} &= \overline{z} - u_2(\overline{x},\overline{y},\overline{z}),\\
D^{\alpha_3}\overline{z} &= -a\overline{x} - b\overline{y} - c\overline{z} + \frac{a\tau_1}{\pi}\sum_{j=-r_1}^{s_1} f'_{1j}(\eta_{1j})\overline{x}\\
&\quad + \frac{b\tau_2}{\pi}\sum_{j=-r_2}^{s_2} f'_{2j}(\eta_{2j})\overline{y} - u_3(\overline{x},\overline{y},\overline{z}),
\end{aligned} \tag{61}$$

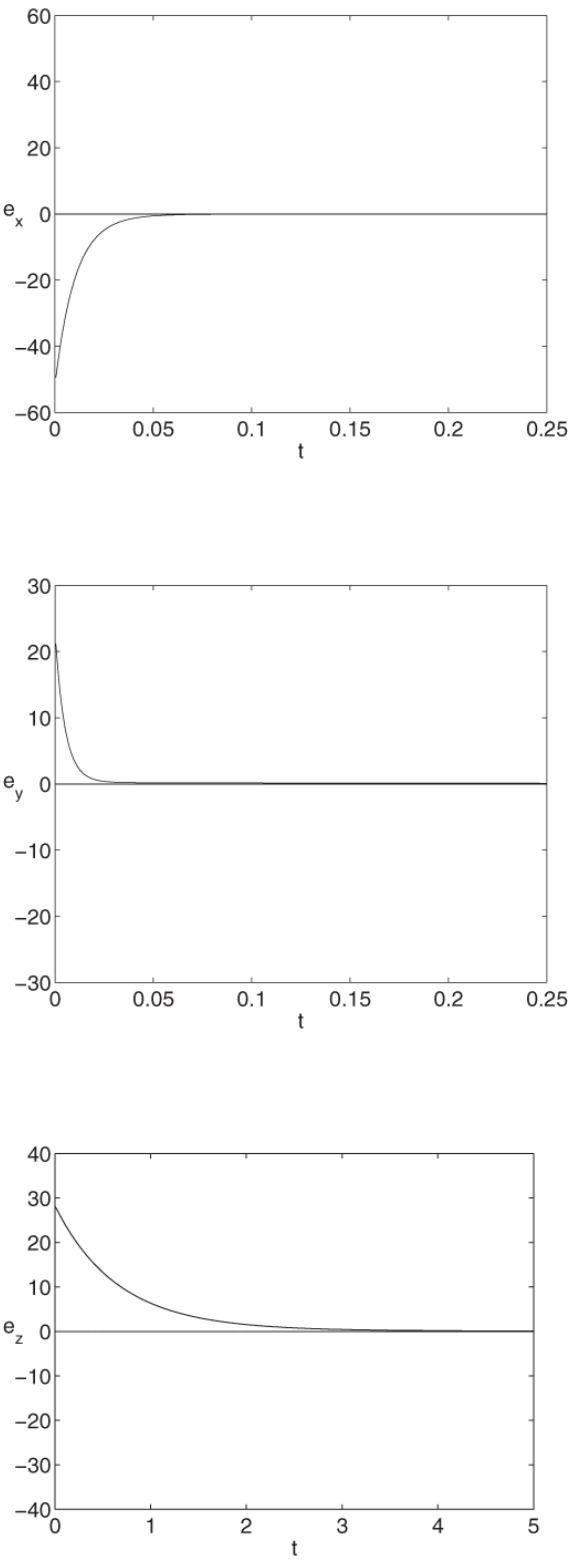

Fig. 21. Time history of the error system (58) for $a = b = c = 0.5$, $r_1 = s_1 = r_2 = s_2 = 1$, $\tau_1 = \tau_2 = 100$, $\alpha_1 = \alpha_2 = \alpha_3 = 0.99$ with the control law given in Theorem 10, using the initial conditions, $x_d(0) = -50$, $y_d(0) = 15$, $z_d(0) = 12$ and $x_r(0) = 2$, $y_r(0) = -8$, $z_r(0) = -16$, when $\delta_x = 90$, $\delta_y = 180$ and $\delta_z = 1$.

then either of the following conditions

(1) $\delta_x > 1 + \dfrac{\tau_2}{\pi}(s_2 + r_2 + 1)$,

$\delta_y > 1$,

$\delta_z > a + \dfrac{a\tau_1}{\pi}(s_1 + r_1 + 1) + b + \dfrac{b\tau_2}{\pi}(s_2 + r_2 + 1) - c$;

(2) $\delta_x > a + \dfrac{a\tau_1}{\pi}(s_1 + r_1 + 1)$,

$\delta_y > 1 + \dfrac{\tau_2}{\pi}(s_2 + r_2 + 1) + b + \dfrac{b\tau_2}{\pi}(s_2 + r_2 + 1)$,

$\delta_z > 1 - c$;

guarantees the stability of $X^* = (x^*, y^*, z^*)$.

The correctness of Corollary 10.2 is verified using numerical simulations. As shown in Fig. 22, with the designed control law, when the first condition of Corollary 10.2 is satisfied with $\delta_x = 150$, $\delta_y = 2$ and $\delta_z = 180$, the solution orbit of system (61) converges to the equilibrium point $(0, 0, 0)$.

10.3. *Synchronization and stabilization of fractional order 3-D-$m \times n \times l$-grid-scroll chaotic attractors*

In this section, we investigate synchronization and stabilization of the fractional order 3-D-$m \times n \times l$-grid-scroll chaotic attractors using simple feedback control laws. We first consider synchronization of two such systems. The driving system can be written as

$$
\begin{aligned}
D^{\alpha_1} x_d(t) &= y_d - \frac{\tau_2}{2}\left[(r_2 - s_2) + \sum_{j=-r_2}^{s_2} \frac{2}{\pi}\tan^{-1}(y_d + j\tau_2)\right],\\
D^{\alpha_2} y_d(t) &= z_d - \frac{\tau_3}{2}\left[(r_3 - s_3) + \sum_{j=-r_3}^{s_3} \frac{2}{\pi}\tan^{-1}(z_d + j\tau_3)\right],\\
D^{\alpha_3} z_d(t) &= -ax_d - by_d - cz_d + \frac{a\tau_1}{2}\left[(r_1 - s_1) + \sum_{j=-r_1}^{s_1} \frac{2}{\pi}\tan^{-1}(x_d + j\tau_1)\right]\\
&\quad + \frac{b\tau_2}{2}\left[(r_2 - s_2) + \sum_{j=-r_2}^{s_2} \frac{2}{\pi}\tan^{-1}(y_d + j\tau_2)\right] + \frac{c\tau_3}{2}\left[(r_3 - s_3) + \sum_{j=-r_2}^{s_2} \frac{2}{\pi}\tan^{-1}(z_d + j\tau_3)\right],
\end{aligned}
\tag{62}
$$

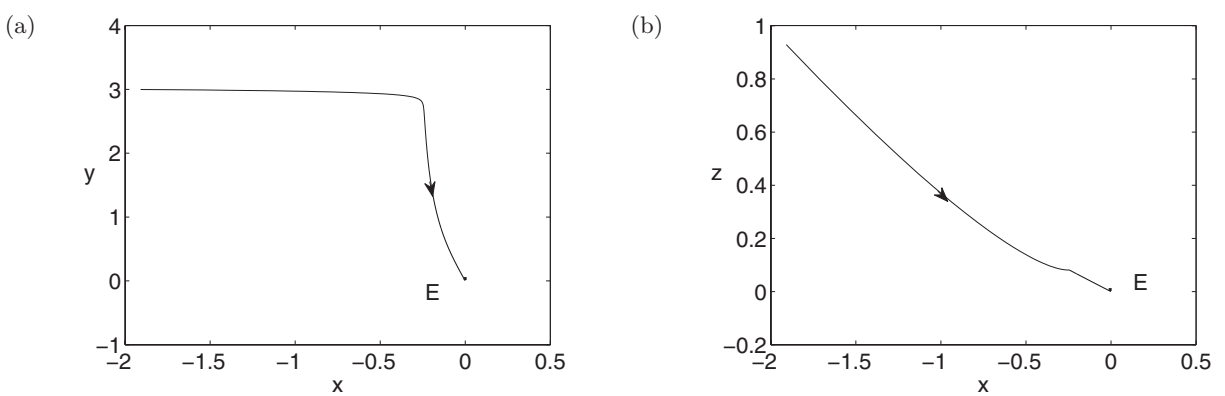

Fig. 22. Trajectory of a 2-D-4 × 4-grid-scroll chaotic attractor for system (61) when $a = b = c = 0.5$, $\tau_1 = \tau_2 = 100$, $r_1 = s_1 = r_2 = s_2 = 1$, $\alpha_1 = \alpha_2 = \alpha_3 = 0.99$ with the control law given in Corollary 10.2 for $\delta_x = 150$, $\delta_y = 2$ and $\delta_z = 180$, convergent to the equilibrium point, $E(0, 0, 0)$: (a) projected on the x–y plane and (b) projected on the x–z plane.

whose corresponding driven system with control law applied is given by

$$\begin{aligned}
D^{\alpha_1}x_r(t) &= y_r - \frac{\tau_2}{2}\left[(r_2 - s_2) + \sum_{j=-r_2}^{s_2}\frac{2}{\pi}\tan^{-1}(y_r + j\tau_2)\right] + u_1(e_x, e_y, e_z),\\
D^{\alpha_2}y_r(t) &= z_r - \frac{\tau_3}{2}\left[(r_3 - s_3) + \sum_{j=-r_3}^{s_3}\frac{2}{\pi}\tan^{-1}(z_r + j\tau_3)\right] + u_3(e_x, e_y, e_z),\\
D^{\alpha_3}z_r(t) &= -ax_r - by_r - cz_r + \frac{a\tau_1}{2}\left[(r_1 - s_1) + \sum_{j=-r_1}^{s_1}\frac{2}{\pi}\tan^{-1}(x_r + j\tau_1)\right]\\
&\quad + \frac{b\tau_2}{2}\left[(r_2 - s_2) + \sum_{j=-r_2}^{s_2}\frac{2}{\pi}\tan^{-1}(y_r + j\tau_2)\right] + \frac{c\tau_3}{2}\left[(r_3 - s_3) + \sum_{j=-r_3}^{s_3}\frac{2}{\pi}\tan^{-1}(z_r + j\tau_3)\right]\\
&\quad + u_3(e_x, e_y, e_z),
\end{aligned} \tag{63}$$

where u_i's are the controls. The difference between the driving system (62) and its corresponding driven system (63) is described by the following error system:

$$\begin{aligned}
D^{\alpha_1}e_x &= e_y - \frac{\tau_2}{\pi}\sum_{j=-r_2}^{s_2} f'_{2j}(\xi_{2j})e_y - u_1(e_x, e_y, e_z),\\
D^{\alpha_2}e_y &= e_z - \frac{\tau_3}{\pi}\sum_{j=-r_3}^{s_3} f'_{3j}(\xi_{3j})e_z - u_2(e_x, e_y, e_z),\\
D^{\alpha_3}e_z &= -ae_x - be_y - ce_z + \frac{a\tau_1}{\pi}\sum_{j=-r_1}^{s_1} f'_{1j}(\xi_{1j})e_x + \frac{b\tau_2}{\pi}\sum_{j=-r_2}^{s_2} f'_{2j}(\xi_{2j})e_y + \frac{c\tau_3}{\pi}\sum_{j=-r_3}^{s_3} f'_{3j}(\xi_{3j})e_z\\
&\quad - u_3(e_x, e_y, e_z).
\end{aligned} \tag{64}$$

Theorem 11. *With the simple linear feedback control law,*

$$u_1 = \delta_x e_x, \quad u_2 = \delta_y e_y, \quad u_3 = \delta_z e_z, \tag{65}$$

applied to system (51), if one of the following conditions,

(1) $\delta_x > 1 + \frac{\tau_2}{\pi}(s_2 + r_2 + 1)$,

$\delta_y > 1 + \frac{\tau_3}{\pi}(s_3 + r_3 + 1)$,

$\delta_z > a + \frac{a\tau_1}{\pi}(s_1 + r_1 + 1) + b + \frac{b\tau_2}{\pi}(s_2 + r_2 + 1) - c + \frac{c\tau_3}{\pi}(s_3 + r_3 + 1)$;

(2) $\delta_x > a + \frac{a\tau_1}{\pi}(s_1 + r_1 + 1)$,

$\delta_y > 1 + \frac{\tau_2}{\pi}(s_2 + r_2 + 1) + b + \frac{b\tau_2}{\pi}(s_2 + r_2 + 1)$,

$\delta_z > 1 - c + \frac{\tau_3}{\pi}(s_3 + r_3 + 1) + \frac{c\tau_3}{\pi}(s_3 + r_3 + 1)$;

holds, then the zero solution of (64) is stabilized, and thus the driving system (62) and the driven system (63) are synchronized.

Proof. The proof is similar to that of Theorem 9, and hence is omitted. ■

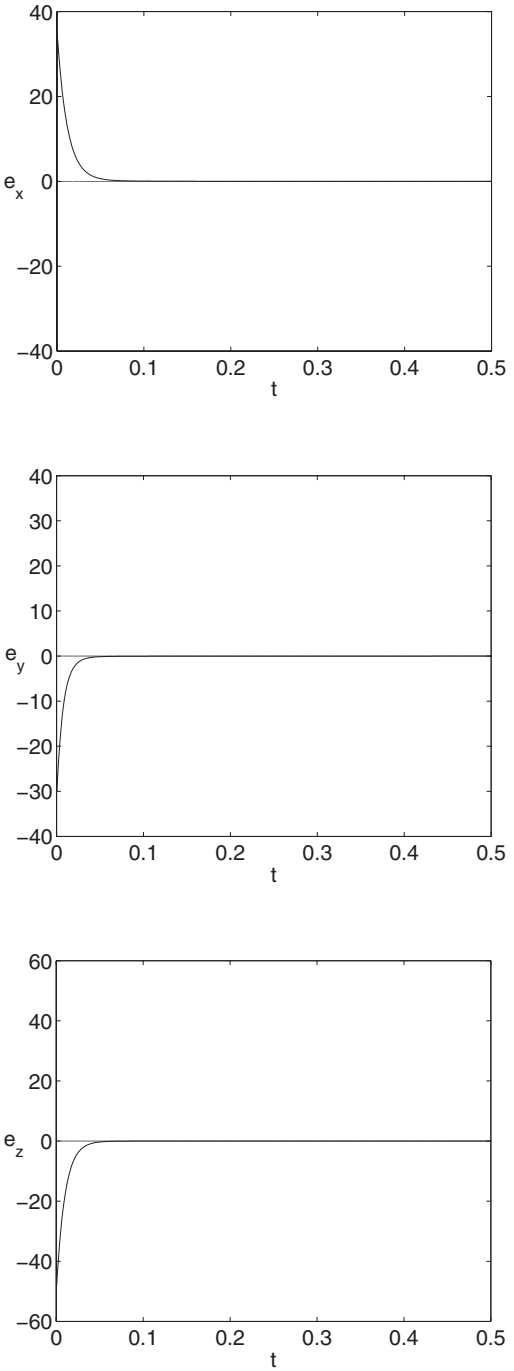

Fig. 23. Time history of the error system (64) for $a = b = c = 0.5$, $r_1 = s_1 = 1$, $r_2 = s_2 = 0$, $r_3 = s_3 = 0$, $\tau_1 = \tau_2 = \tau_3 = 100$, $\alpha_1 = \alpha_2 = 0.99$, $\alpha_3 = 0.998$ with the control law given in Theorem 11, using the initial conditions, $x_d(0) = 30$, $y_d(0) = -29$, $z_d(0) = -18$ and $x_r(0) = -6$, $y_r(0) = 3$, $z_r(0) = 32$, when $\delta_x = 80$, $\delta_y = 120$ and $\delta_z = 100$.

Next, we use numerical simulation to verify the applicability of Theorem 11. Under the proposed control law with $\delta_x = 80$, $\delta_y = 120$ and $\delta_z = 100$ (i.e. the second condition of Theorem 11 is satisfied), the zero solution of system (64) is stabilized and hence the synchronization of systems (62) and (63) is realized.

Corollary 10.3. *With the feedback control law*

$$u_1 = \delta_x \overline{x}, \quad u_2 = \delta_y \overline{y}, \quad u_3 = \delta_z \overline{z} \tag{66}$$

applied to system

$$\begin{aligned}
D^{\alpha_1}\overline{x} &= -\delta_x \overline{x} + \overline{y} - \frac{\tau_2}{\pi} \sum_{j=-r_2}^{s_2} f'_{2j}(\eta_{2j})\overline{y},\\
D^{\alpha_2}\overline{y} &= -\delta_y \overline{y} - \frac{\tau_3}{\pi} \sum_{j=-r_3}^{s_3} f'_{3j}(\eta_{3j})\overline{z},\\
D^{\alpha_3}\overline{z} &= -(\delta_z + c)\overline{z} - a\overline{x} - b\overline{y}\\
&\quad + \frac{a\tau_1}{\pi} \sum_{j=-r_1}^{s_1} f'_{1j}(\eta_{1j})\overline{x}\\
&\quad + \frac{b\tau_2}{\pi} \sum_{j=-r_2}^{s_2} f'_{2j}(\eta_{2j})\overline{y}\\
&\quad + \frac{c\tau_3}{\pi} \sum_{j=-r_3}^{s_3} f'_{3j}(\eta_{3j})\overline{z},
\end{aligned} \tag{67}$$

for any given equilibrium $X = X^*$, if one of the following conditions

(1) $\delta_x > 1 + \dfrac{\tau_2}{\pi}(s_2 + r_2 + 1)$,

$\delta_y > 1 + \dfrac{\tau_3}{\pi}(s_3 + r_3 + 1)$,

$\delta_z > a + \dfrac{a\tau_1}{\pi}(s_1 + r_1 + 1) + b$

$+ \dfrac{b\tau_2}{\pi}(s_2 + r_2 + 1) - c$

$+ \dfrac{c\tau_3}{\pi}(s_3 + r_3 + 1)$;

(2) $\delta_x > a + \dfrac{a\tau_1}{\pi}(s_1 + r_1 + 1)$,

$\delta_y > 1 + \dfrac{\tau_2}{\pi}(s_2 + r_2 + 1) + b$

$+ \dfrac{b\tau_2}{\pi}(s_2 + r_2 + 1)$,

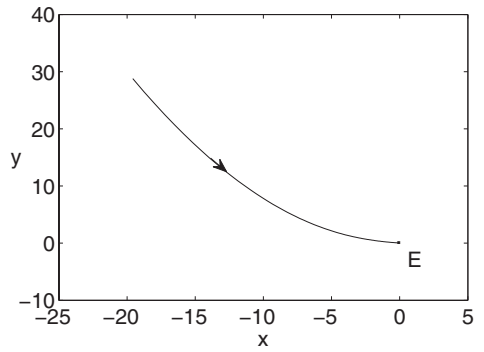

(a)

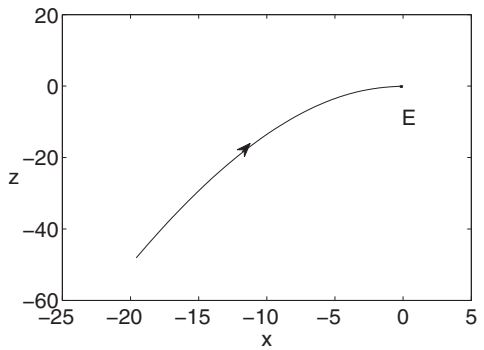

(b)

Fig. 24. Trajectory of a 3-D-4 × 2 × 2-grid-scroll chaotic attractor for system (67) when $a = b = c = 0.5$, $\tau_1 = \tau_2 = \tau_3 = 100$, $r_1 = s_1 = 1$, $r_2 = s_2 = r_3 = s_3 = 0$, $\alpha_1 = \alpha_2 = 0.99$, $\alpha_3 = 0.998$ with the control law given in Corollary 10.3 for $\delta_x = 80$, $\delta_y = 150$ and $\delta_z = 150$, convergent to the equilibrium point, $E(0, 0, 0)$: (a) projected on the x–y plane and (b) projected on the x–z plane.

$$\delta_z > 1 - c + \frac{\tau_3}{\pi}(s_3 + r_3 + 1) + \frac{c\tau_3}{\pi}(s_3 + r_3 + 1);$$

is satisfied, then $X^* = (x^*, y^*, z^*)$ *is stabilized.*

To illustrate the use of Corollary 10.3, we present a numerical example. Take $\delta_x = 80$, $\delta_y = 150$ and $\delta_z = 150$, which satisfy the first condition of Corollary 10.3. Thus, under the constructed control law, the trajectory of system (67) converges to the equilibrium point $(0, 0, 0)$, as shown in Fig. 24.

11. Conclusions

In this article, we have applied the $\tan^{-1}(x)$ function series to generate 1-D-n-scroll, 2-D-$m \times n$-grid-scroll and 3-D-$m \times n \times l$-grid-scroll with integer order or fractional order, chaotic attractors. The systems considered in this paper can generate chaotic attractors with any number (≥ 2) of chaotic scrolls. The maximal number of the scrolls in the x, y or z coordinate can be regulated by changing two coefficients r_i and s_i in the corresponding $\tan^{-1}(x)$ function series. Moreover, we design simple feedback control laws to study stabilization and synchronization for one-directional, two-directional and three-directional multi-scroll integer order and fractional order chaotic attractors. Based on the structure of the system, simple feedback control laws are constructed to synchronize or stabilize such integer order and fractional order chaotic systems. Numerical simulations are presented to validate the effectiveness and applicability of the proposed control laws.

Acknowledgments

This work was supported by the Natural Sciences and Engineering Research Council of Canada (NSERC, No. R2686A02) and the National Natural Science Foundation of China (NNSFC, Nos. 60274007 and 60474011).

References

Ahmed, E., El-Sayed, A. & Elsaka, H. [2007] "Equilibrium points, stability and numerical solutions of fractional-order predator-prey and rabies models," *J. Math. Anal. Appl.* **325**, 542–553.

Cafagna, D. & Grassi, G. [2003] "New 3-D-scroll attractors in hyperchaotic Chua's circuit forming a ring," *Int. J. Bifurcation and Chaos* **13**, 2889–2903.

Chen, G. R. & Ueta, T. [1999] "Yet another chaotic attractor," *Int. J. Bifurcation and Chaos* **9**, 1465–1466.

Chua, L. O., Komuro, M. & Matsumoto, T. [1986] "The double scroll family," *IEEE Trans. Circuits Syst.* **33**, 1072–1118.

Forti, M. [2002] "Some extensions of a new method to analyze complete stability of neural networks," *IEEE Trans. Neural Networks* **13**, 1230–1238.

Huang, X., Zhao, Z., Wang, Z. & Li, Y. X. [2012] "Chaos and hyperchaos in fractional-order cellular neural networks," *Neurocomputing* **94**, 13–21.

Li, C. G. & Chen, G. R. [2004] "Chaos and hyperchaos in the fractional-order Rössler equations," *Physica A* **341**, 55–61.

Liao, X. X. [2001] *Mathematical Theory and Application of Stability*, 2nd edition (Central China Normal University Press, Wuhan, China).

Lorenz, E. N. [1963] "Nonperiodic flow," *J. Atmos. Sci.* **20**, 130–141.

Lü, J. H., Chen, G. R., Yu, X. H. & Leung, H. [2004] "Design and analysis of multi-scroll chaotic attractors from saturated function series," *IEEE Trans. Circuits Syst.-I* **51**, 2476–2490.

Lu, J. G. & Chen, G. R. [2006] "A note on the fractional-order Chen system," *Chaos Solit. Fract.* **27**, 685–688.

Matignon, D. [1996] "Stability results for fractional differential equations with application to control processing, in: Computational engineering in system application," *IMACS-SMC*, *Lille*, *France* **2**, 963–968.

Rössler, O. E. [1976] "An equation for continuous chaos," *Phys. Lett. A* **57**, 397–398.

Wu, X., Li, J. & Chen, G. R. [2008] "Chaos in the fractional order unified system and its synchronization," *J. Franklin Instit.* **345**, 392–401.

Xu, F., Shu, X. B. & Cressman, R. [2013] "Chaos control and chaos synchronization of fractional order smooth Chua's system," *Dyn. Contin. Discr. Impuls. Syst., Ser. B Appl. Algorith.* **20**, 117–133.

Yalcin, M. E., Suykens, J. A. K. & Vandewalle, J. [1999] "On the realization of n-scroll attractors," *Proc. 1999 IEEE Int. Symp. Circuits Syst.* (*ISCAS*) **5**, 483–486.

Yu, S. M., Lü, J. H., Leung, H. & Chen, G. R. [2005] "Design and implementation of n-scroll chaotic attractors from a general jerk circuit," *IEEE Trans. Circuits Syst.-I* **52**, 1459–1476.

Zhang, C. X. & Yu, S. M. [2010] "Generation of grid multi-scroll chaotic attractors via switching piecewise linear controller," *Phys. Lett. A* **374**, 3029–3037.

Zhang, K., Wang, H. & Fang, H. [2012] "Feedback control and hybrid projective synchronization of a fractional-order Newton–Leipnik system," *Commun. Nonlin. Sci. Numer. Simulat.* **17**, 317–328.